Octadecyltrichlorosilane (OTS) deposited films obtained under various conditions. A protocol to produce high-quality OTS films with potential applications in metal-insulator-metal (MIM) diodes.

ISLAS-GUTIERREZ, SUSANA,STEPHANIE

Octadecyltrichlorosilane (OTS) deposited films obtained under various conditions. A protocol to produce high-quality OTS films with potential applications in metal-insulator-metal (MIM) diodes.

Susana Stephanie Islas-Gutiérrez

A Thesis presented for the degree of
Master of Science

Department of Engineering
University of Durham
2021

Octadecyltrichlorosilane (OTS) deposited films obtained under various conditions and their characterisation using atomic force microscopy (AFM). A protocol to produce high-quality OTS films with potential applications in metal-insulator-metal (MIM) diodes.

Susana Stephanie Islas-Gutiérrez

2021

ABSTRACT

One of the main challenges in the fabrication process of MIM diodes is the ultra-thin thickness and uniformity required in their insulating layer. Currently, there are high-cost processes used to achieve these requirements, but a reliable and low-cost method needs to be developed. Semiconductor's research has described the use of self-assembling organic molecules in MIM diodes due to their ability to form uniform layers, whose thickness and properties can be tailored depending on the functional groups and carbon chain present in the molecule used. Therefore, in this work, octadecyltrichlorosilane (OTS) films deposited on silicon substrates under different conditions were evaluated to determine which factors promote a high-quality monolayer structure on them to design a protocol to be used during the fabrication of MIM diodes using OTS as a dielectric layer. OTS films were produced following the wet chemical coating method and it was found that maturation time, immersion time and temperature are relevant factors to produce monolayers with potential applications as dielectric material. Furthermore, a protocol is described that indicates a maturation time in OTS solution of 30 min, a reaction (immersion) time of 60 min and an immediate baking step at 90°C for 5 min, conditions that favour the formation of monolayers of 2.4 ± 0.4nm thickness. However, further research is needed to test OTS films as dielectric material and to find correlation between monolayer quality and I-V characteristics of MIM diodes.

Key words: MIM diode, SAMs, insulator, dielectric layer, OTS monolayer, wet-chemical coating.

DECLARATION

The work in this thesis is based on joint research carried out at the Department of Engineering, University of Durham, England. No part of this thesis has been submitted elsewhere for any other degree or qualification in this or any other institution, and it is all my own work unless referenced to the contrary in the text.

ACKNOWLEDGEMENTS

Firstly, I would like to express my sincere gratitude to my supervisors Claudio Balocco and Andrew Gallant for the continuous support of my Master and related research, for their patience, motivation and feedback which incentivized me to widen my research from various perspectives. Their guidance helped to encourage my autonomy, to embrace my creativity, to build my character, abilities that will be very useful throughout my life.

In addition, I would like to thank Ian Garrett and Chris Pearson, for their insightful comments and encouragement, to believe in me and strengthen my self-confidence, without their precious emotional and technical support it would not have been possible to conduct this research. Specials thanks to Ellie Desmond who proofread my work.

My sincere thanks also to Jidong Jin and Douglas Uke, who provided me an opportunity to join the “MIM diode world”, to learn from their experience and who gave me access to the laboratory and research facilities.

I thank my fellow lab mates Iman, Polly, Rhiannon, and Rui who made me feel part of the clean-room team, for their advice, friendship and for all the fun we had.

Last but not the least, I would like to thank the Engineering Department at Durham University for all the support and facilities that were provided to me to achieve this research.

DEDICATION

I want to dedicate this research to my parents Leonardo y Marie, because thanks to their wonderful support, their motivating words, and their endless advice I achieved this goal in my life with tremendous learning and great abilities to perform successfully in life. I love you, thank you for always encouraging me with the desire for curiosity.

Thank you for believing in me, for being excited about me, for teaching me that I can achieve everything in life with perseverance, commitment, and determination. I will reach new challenging adventures so that together we can discover the world from different perspectives and keep learning and growing as human beings.

“Around here, however, we don't look backwards for very long. We keep moving forward, opening up new doors and doing new things… and curiosity keeps leading us down new paths.”

W. Disney

CONTENT

1. BACKGROUND

1.1 RESEARCH MOTIVATION

One of the main challenges in the fabrication process of MIM diodes is the ultra-thin thickness and uniformity required in the insulator layer. There are processes as Atomic layer deposition that are used to achieve these requirements however, it is necessary to develop a reliable and low-cost protocol considering the critical dependence of MIM diode performance on small variations of its insulator.

Recently, research has described the use of self-assembling organic molecules in electronics [1-4] due to their ability to form uniform layers, whose thickness and properties can be tailored depending on the functional groups present in the molecule used. Studies have described the use of this molecules as dielectrics in the fabrication of MIM diodes due to their ease to form spontaneous monolayers with easy chemical reactions.

An example of this is the work of Etor et al. [5,6] and Jin et al. [7], who are currently working on the fabrication of MIM diodes using self-assembled organic molecules as an insulator. The technique of coating on diodes is quite simple and can be developed at room temperature, however the behaviour of spontaneously self-assembled molecules can be controlled through temperature.

Motivated by this, this work evaluates the formation of monolayers of OTS molecules on silicon substrates under different conditions to determine which conditions promote a high-quality monolayer to generate a potential material for MIM diode fabrication.

1.2 AIM AND OBJECTIVES

The aim of this project was to identify relevant factors during OTS film production that could determine the quality of OTS monolayers with the purpose to design a protocol to be used during MIM diodes fabrication using OTS as dielectric layer.

To reach this, the main objectives are:

- Identify relevant aspects in OTS film deposition that impacts in the formation of monolayers.
- Determine which conditions stimulate a better uniformity in the monolayer.
- Design a temperature control system to tailor OTS deposition conditions to defined temperature regimes.
- Evaluate the OTS monolayers at different reaction conditions.
- Characterise the monolayer of OTS films obtained.
- Design a protocol which have the potential to produce high-quality monolayer films to be used in MIM diodes fabrication.
- Fabricate a MIM diode with OTS as dielectric material.

This last objective could not be met due to the conditions raised worldwide by the COVID-19 virus that stopped the process of experimentation in this work. However, this thesis leaves a precedent for future research that produce more experimentation with OTS films to obtain high-quality monolayers and proceed with further characterization techniques to draw firm conclusions with the purpose to fabricate MIM diodes using high-quality OTS films as dielectric material.

1.3 HYPOTHESIS

Factors as temperature and reaction time during OTS film deposition can influence molecular arrangement to produce uniform and low thickness monolayers, these monolayers described as high-quality might have potential applications as dielectric material in the fabrication of MIM diodes.

The next statements are some assumptions that we have proposed according to the literature:

- The reaction temperature has a relevant influence on the quality of the monolayer [8-10].
- Low temperatures promote a better nucleation and aggregation of OTS molecules in the substrate and hence a better monolayer growth [9,10,11].
- A better quality of OTS monolayer will improve the asymmetry and non-linearity in the diode rectification performance [12,13].

1.4 INTRODUCTION

The exploitation of self-assembled monolayers for electronics arose from the need for novel fabrication techniques to enable miniaturisation of current technology. Modern technology requires smaller devices that work faster, where the integration of a group of molecules or a single molecule just a few nanometres in size works with a specific electronic functionality.

The ease of use of self-assembled molecules lies not only in their ability to coat electrode surfaces with tailored properties, but also in the spontaneous formation of monolayers on a desired surface [14,15], a property valued in the semiconductor industry due to the need for uniform, low-thickness films.

The property of generating monolayers based on self-assembled organic molecules has been reported in the work of Etor et al. [5,6] and Jin et al. [7], who use octadecyltrichlorosilane (OTS) molecules to produce films that function as dielectric material in the fabrication of MIM diodes. The coating method used in their research is a wet chemical adsorption process whereby a pre-treated material is immersed in a solution of organic molecules and, after a time of rest, the monolayer is deduced to be formed. However, interest in exploring different conditions in this wet chemistry method could develop OTS films more suitable for MIM diode fabrication.

Therefore, it is necessary to understand what processes are involved during the self-assembly of OTS molecules and what factors are relevant to develop a better recipe producing reproducible, high quality OTS films for their use as dielectric layers in MIM diode fabrication.

Theoretically, MIM diodes rectification performance can be enhanced by physical parameters such as low thickness and uniformity of their dielectric layer, so the knowledge of the molecular processes involved in the formation of OTS monolayers can guide us to decrease morphological variations in OTs films, i.e., atomic stacking and pinholes, and improve quality of the OTS dielectric layer in MIM diodes.

2. SELF-ASSEMBLED MONOLAYERS (SAMS)

These types of organic molecules are defined as self-assembled due to their spontaneous adsorption on suitable substrates. The assembly process can adopt highly ordered and tightly packed structures, reminiscent of crystalline structures, determined by the chemical structure of the organic molecule itself [16].

The typical structure in self-assembled molecules (SAMs) is described in three main parts, an anchoring group or head, an aliphatic carbon chain or spacer group, and a functional group also called the terminal group or tail. These three main parts are responsible for the packing structure that forms into monolayers. The schematic representation is illustrated in Fig. 8.

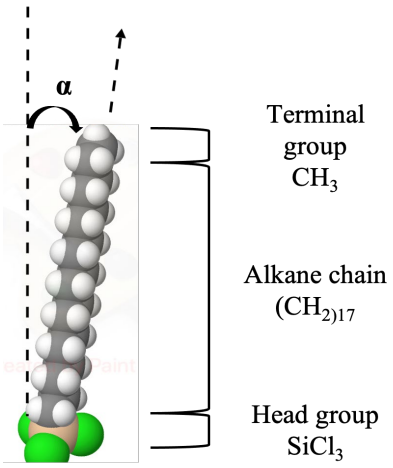

Fig. 8. Model of a self-assembled molecule represented with Van der Waals spheres. These spheres represent the surface through which the molecule interacts with other molecules under a certain angle (α) which depends on the aliphatic chain. [17].

The process of formation of these monolayers is spontaneously generated and their arrangement is driven by the adsorption process which, according to Ulman [18], is a two-step process: the covalent bonding of the anchoring chemical group (adsorbate) to the surface (substrate) and the intermolecular interactions, i.e., the Van der Waals forces of the aliphatic carbon chain between the self-assembled pieces of molecules.

The chemical affinity between the adsorbate and the substrate provides a driving force to fill all the sites on the substrate surface and displace contaminants from the substrate. Once the adsorption sites on the surface are filled, the chains will be close enough that the weaker Van der Waals interactive forces between the chains can exert their influence and lead to crystallisation of the SAM molecules and formation of monolayers.

Examples of adsorbate-substrate pairs commonly used to generate SAMs are (i) carboxylic acids on aluminium or silver oxide, (ii) alcohols, amines and isonitriles on platinum, (iii) dialkyl sulphides and dialkyl disulphides on gold, (iv) alkane thiols on metals such as gold, silver and copper, and non-metals such as GaAs, InP and indium tin oxide, and (v) organosilane derivatives on hydroxylated surfaces, the latter being of interest for the development of this work.

2.1 OCTADECYLTRICHLOROSILANE (OTS) MOLECULE

Organosilane derivatives belong to a family which anchor group is a silane (Si) attached to three chlorine atoms (Cl_3); commonly this anchor head adsorbates on hydroxylated substrates i.e., hydroxyl (-OH) groups presents on substrate surface. Its use was first reported by Bigelow et al. [19] and since then is widely reported in formation of SAMs on oxidised silicon surfaces [5,14,20-22] and widely used in semiconductor industry.

There are many trichlorosilane molecules which have varying chain lengths but the one used in this project is octadecyltrichlorosilane (OTS) that has eighteen carbon (C18), an oriented array (α) at $\sim$30º, and its structural chemical formula $C_{18}H_{37}SiCl_3$ is schematised in Fig.10.

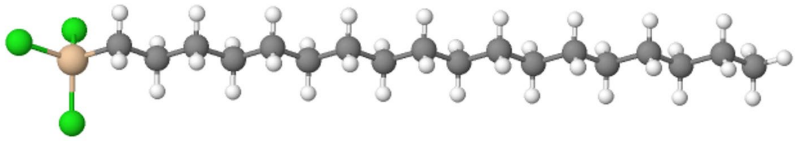

Fig. 10. Octadecyltrichlorosilane (OTS) model represented with balls and sticks to emphasise the atoms and their bonds. The silicon head group is marked in gold and green ($SiCl_3$), the eighteen carbon atoms in grey and oxygens in white.

The OTS monolayers produced have a typical thickness of approximately 2 nm [22-24]. Fig. 11 illustrates OTS molecules bonded covalently to substrate where closely packed order is determined by its tilt (α) at ~30º [14].

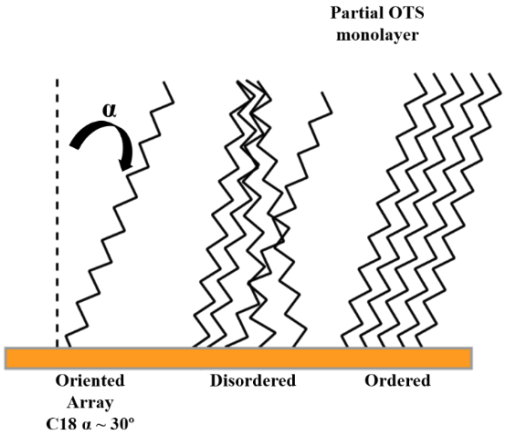

Fig. 11. Schematic representation of OTS partial monolayer with ordered and disordered molecules attached to the substrate.

The deposition method by which monolayers of OTS are generated is called wet-chemical coating and at the molecular level the anchor, or OTS head group ($-SiCl_3$) is responsible for the adsorption of the molecule to the hydroxylated surface; while the long alkyl chain of methylene groups $(-CH_2)_{17}$ determines the intermolecular interaction that promotes ordering and orientation of SAM molecules within the monolayer and finally, the terminal methyl surface group $-(CH_3)$ determines surface properties, being a non-polar group gives hydrophobic properties to the surface coated [11].

2.2 WET CHEMICAL OTS COATING METHOD

The wet-chemical coating method is used as a method for OTS film deposition in which at molecular level, adsorption, self-assembly and covalent bonding attach the molecules onto the silicon oxide wafer, while in “bulk level” a coating material usually silica is pre-treated to present a thin adsorbed water layer and immersed into a solution of organic self-assembling molecules and finally after a period of time, the sample is cleaned and baked for the film settling onto the surface of the coated material.

During this procedure, there are several factors can affect monolayer structure leading to pinhole defects which are undesirable to electronic applications [25], these are cleanliness and humidity of the setup [20,26], purity of the chemicals and solvent use [27,28], concentration of the molecules into solution [29,30], temperature of the solution [8-10,28,31], maturation and immersion time of the substrate [8,11,32-34]. The following paragraphs review each of the factors that can affect the monolayer structure of OTS films.

The setup and substrate cleanliness are essential to avoid introducing particles into the OTS solution that would affect the monolayer structure for which strong oxidising solutions (such as piranha solution) or an oxygen plasma are used to restore surface quality of substrate and materials involved in coating technique [21].

Research indicates that type of solvent directly affects the kinetics of assembly at molecular level, Dannenberger et al. [27] reported low viscosity solvents favour kinetics speed and Rozlosnik et al. [28] remarked solvent selection may influence monolayer or multilayer formation, however there is no concise information for OTS films. However, OTS/solvent solution is commonly prepared with low toxicity, low cost, and high purity liquid solvents such as alkanes (hexane, heptane, hexadecane), alcohols (ethanol), cyclohexane and toluene [35], at an OTS solute concentration typically 10^{-3} M but can vary from 10^{-1} M to 10^{-4} M [29,30]. In addition, is reported that adding carbon tetrachloride (-CCl_4) or 1-dodecanethiol to the medium favour solubility of the polar head group [5,7,8,11,16,21,22,26].

2.3 TEMPERATURE IN OTS COATING

Most of the literature describes wet-coating method at room temperature (20°C-25°C), but temperature range in self-assembly molecules varies from -20°C to around 80°C [6] this temperature range is due to an intrinsic relationship between chain length and temperature required for the formation of an ordered monolayer, the smaller the chain length the lower the temperature required [8,9,28].

Temperature has been reported as an important factor to obtain reproducible and uniform monolayers. Desbief et al. [11] stated that the formation of ordered monolayers is easily achieve in low temperatures below 20°C, whereas Goswami et al. [36] reported that monolayer is achieved at higher temperatures above 25°C.

Brzoska et al. [8] have pointed out the existence of a transition temperature which controls the monolayer's formation of silane molecules on hydrophilic substrates, below this temperature layers of high surface quality are obtained, and this transition temperature linearly increases with the alkyl-chain-length and it is independent of the nature of the solvents used for the reaction.

The discrepancy between high or low temperatures to promote better assembly kinetics at the molecular level and thus, higher probability of forming monolayers lies in different theories to explain OTS monolayer formation.

The thermodynamic theory states the coexistence of different phases (molecular arrangements) at different temperatures. At high temperatures, the monolayer state can change from a gas (G) i.e., molecules widely separated, to a liquid expanded (LE) phase i.e., molecules packed together in a random fashion, and further on as temperature increases the molecular density increases as well and it reaches a liquid condensed (LC) phase i.e., molecules held in a fixed pattern. On the other hand, at low temperatures, the LE phase is missing, and the G phase is directly followed by the LC phase [8,37].

This transition temperature is supported by Carraro et al. [10] who studied the growth of OTS-SAMs and reported the existence of two critical temperatures, reaffirming Brzoska et al. [8] model: the LE mode, by formation of a homogeneous and disordered monolayer at high temperatures; the CL mode, by formation of dense and ordered islands at low temperatures, and the coexistence of those two growth modes (EL+CL) at intermediate temperatures.

The target using OTS as dielectric is to create the LC phase at low temperatures which is described as closely packed and well-ordered (fully stretched in their all-trans conformation), while the LE and G phases contain many “gauche defects” [8].

The elimination of “gauche defects” is essential to obtain a high-quality monolayer however, Aswal et al. [14,15] and Bierbaum et al. [38] have indicated the growth kinetics as a function of chain length affirmed that long chains grow via island nucleation and because of this, the complete elimination of pinholes is impossible to control in molecules with long chains.

On the other hand, self-assembly process can be explained through the different chemical reactions involved in the process, in the next section is discussed the reactions proposed in this theory.

2.4 OTS COATING AT MOLECULAR LEVEL

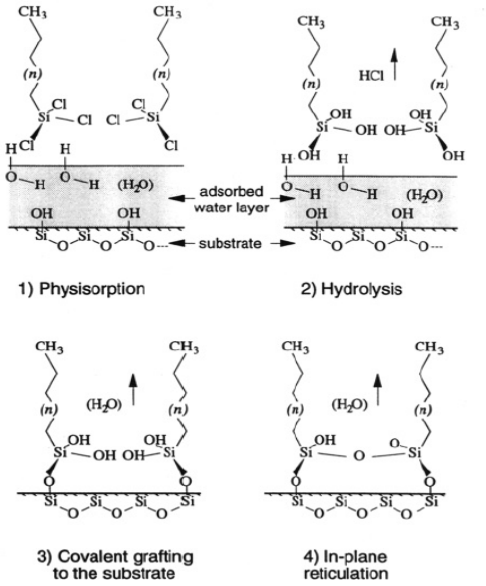

Fig. 9. General scheme proposed for SAM formation in wet conditions [4].

To explain the wet chemical method at molecular level Fig. 9 describes 4 main steps and reactions. The step 1) physisorption, happens during substrate pre-treatment when a thin adsorbed water film is created onto substrate surface. At molecular level this step represents the addition of hydroxyl groups (-OH) (i.e., hydroxylation) in substrate to allow easy diffusion of OTS molecules and to assure anchoring sites for assembly. It has been reported morphological variations in OTS monolayers on silicon dioxide as a substrate as consequence to the hydroxyl groups density in the substrate surface [32] and the hydration degree in the atomic surface and bulk [11,16,32].

The next steps 2) hydrolysis and 3) covalent grafting are known as silanisation reactions and happen when substrate is immersed into OTS/solvent solution and still during certain time. The added hydroxyl groups (-OH) to substrate surface lead the covalent binding of the silicon (Si) with the hydroxylated substrate, eliminating hydrogen groups (i. e., hydrolysis) in form of chloric acid (HCl). These reactions are water and air sensitivity due to oxygen bridge bonds between the organic OTS layer and the inorganic substrate and must be conducted under inert conditions in strictly anhydrous medium.

Caution in this step is crucial for monolayer formation because any contact with water, produces an effect called cross-linking, in which not only the anchor heads of OTS molecules are part of the reaction, but the carbon chain reacts linking themselves with other carbon chains preventing OTS molecules moves freely and being deposited in an orderly fashion on the substrate.

Finally step 4) in-plane reticulation, happens once substrate is thoroughly rinsed in organic solvents to remove any physical adsorbed molecules from the substrate and subjected to an annealing process (i.e., baking) at temperatures above 90°C to evaporate remaining solvent and water, giving stability to newly formed covalent bonds. OTS film formation can be verified through the hydrophobicity of the substrate, initially hydrophilic in the activation process.

As seen in the 4 steps above, the process of forming monolayers with self-assembling molecules is not complex, and although it is well described in literature, there is no mention of the role of temperature or immersion time in the process, so there is an area of opportunity for research.

On the other hand, the relevance of being able to deposit OTS films that are monolayer structures at the molecular level is that their use in MIM diodes requires compliance with certain characteristics that have not been reported so far in the research on the use of OTS molecules.

As we will see below during the MIM diode fabrication process as reported in Jin et. al. [7] OTS deposition is performed at room temperature. However, manipulation of factors such as temperature and immersion time could help to improve the fabrication quality of MIM diodes. It is well known that deposition method can have a strong influence on electrical properties, because MIM operation should be based on tunnelling and this is exponentially dependent on the barrier thickness due to this extremely uniform thickness control of the ultrathin insulating layer is required.

2.5 OTS FILMS IN MIM DIODES

Understanding the fabrication of MIM diodes is essential to pursue improvements in the adsorption of the insulator layer and determine the experimentation required to accomplish low thickness and uniformity using organic molecules that assemble spontaneously on surfaces by adsorption [39].

The method used to fabricate MIM diodes is described by Jin et al. [7] which in turn leads to the article of Etor et al. [5]. The MIM diodes are fabricated with dissimilar work function metals, Titanium (4.33 eV) and Platinum (5.65 eV), which have a work function difference of 1.4 eV that exhibits a strong non-linear current-voltage (J-V) characteristic.

MIM diodes are fabricated on 2-inch silicon wafers with a 300 nm thermally grown SiO_2 layer and the first step in MIM diodes fabrication (Fig 12a) is to create a bilayer of approximately 25 nm of titanium (Ti) coated with 80 nm of gold (Au) deposited by e-beam evaporation and lifted off. The evaporation system used for the metal deposition is in a Moorfield minilab 060 e-beam evaporator (Moorfield Nanotechnology Ltd., Cheshire, UK).

After a photolithographic patterning step (Fig 12c and 12d), gold is removed by an iodine/iodide wet etching, leaving some regions of titanium exposed (Fig. 12d). Then, the exposed titanium is coated with OTS following wet-chemical coating method at room temperature (Fig. e).

Finally, a thin layer of platinum (Pt) with a nominal thickness of 80 nm is evaporated (Fig. f) and lift off in the unexposed regions, resulting in Ti/OTS/Pt junctions (Fig. 12g). The defined MIM junction is determined using 2 masks and the overlapping region between the Ti and Pt contacts determined the effective area of the diode.

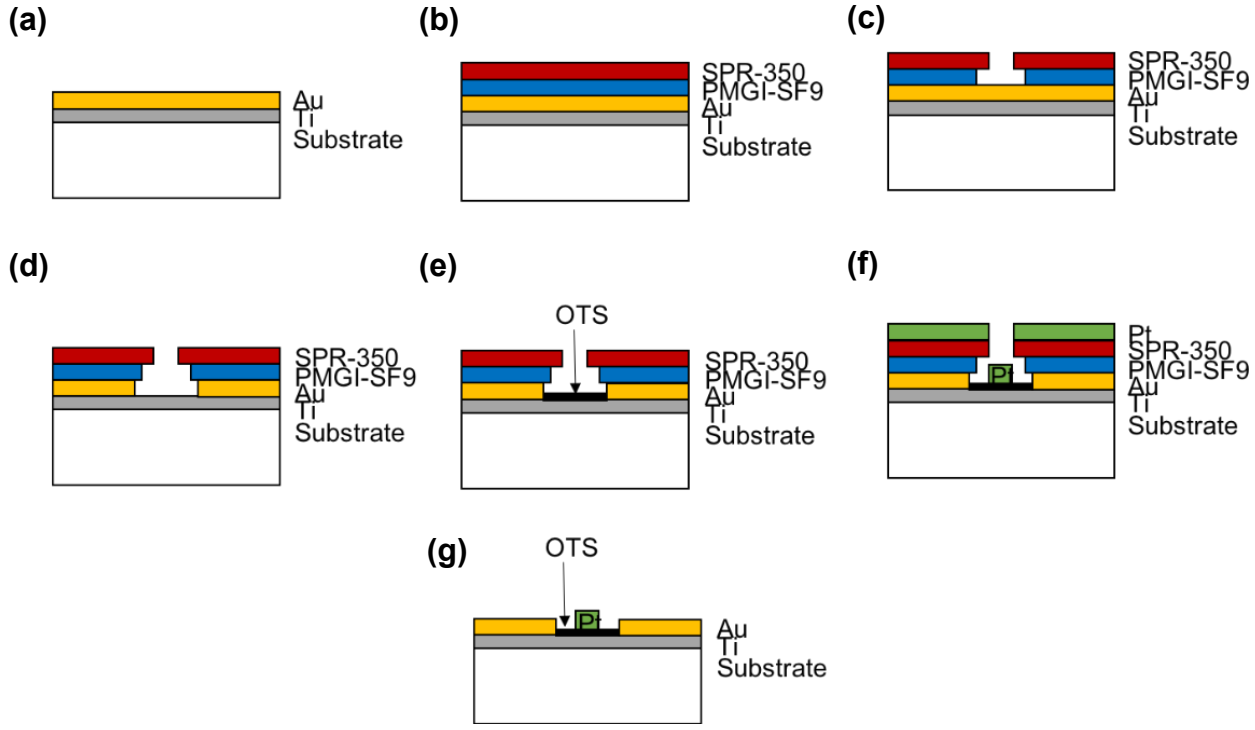

Fig. 12. Schematic of MIM diode fabrication based on Jin et al. [7].

Analysing MIM diode fabrication procedure it is remarkable that quantities of metals used are on the nanometre scale and with the help of e-beam evaporator it is ensure that the right quantities are added to the substrate. However, they neglect this same precision in the OTS coating process when the theory of MIM diodes states that the insulation should be ultralow thickness and uniformity.

Research has been developed about the application of self-assembly molecules as dielectric in electronics or as an insulator layer for tunnel diodes and rectifiers for rectenna applications [5,7,20,21,34]. Although, systematic experimental studies to correlate the morphology of the films produced using SAMs to MIM rectification performance have been largely absent. The next section of this work will discuss the theory behind MIM diodes and the relevance of the OTS film quality in MIM diodes performance.

3. MIM DIODE

3.1 INTRODUCTION

The Metal-Insulator-Metal (MIM) diode (Fig. 1) is a thin-film device described as an ultra-thin insulator layer stacked between two similar or dissimilar metal electrodes [40].

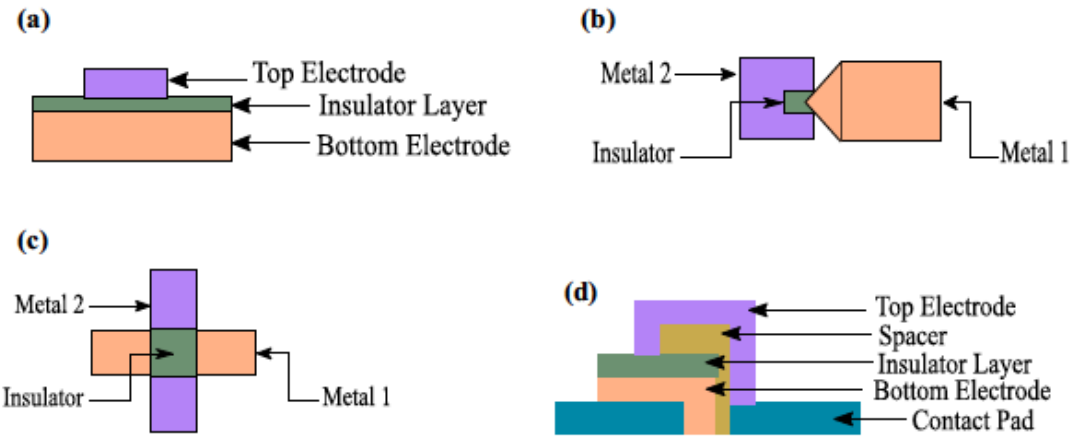

Fig. 1. Schematic of different structures of MIM diodes (a) stacked structure, (b) manually aligned, (c) self-aligned stepped structure and (d) spaced stepped structure [41].

Current transport in MIM diodes is due to quantum-tunnelling [42] in which transmission of an electron wave function between the electrodes occurs via penetrating the energy gap of the insulator barrier [43,44]. The transmitted wave tunnels through the barrier with the same frequency, but the amplitude attenuates (Fig. 2) due to reflections at the interfaces [42]. The quantum-tunnelling conduction in MIM diodes facilitates ultrafast switching speed (i.e., 0.3-430 THz IR frequencies) beyond the conventional high-frequency GaAs Schottky diodes whose cut-off frequency operation is limited to only a few terahertz [45, 46].

Furthermore, MIM diodes also exhibit many other advantages, such as miniature size and simple architecture, very broad bandwidth, ease of integration with Complementary Metal Oxide Semiconductor (CMOS) technology [42]. These features

contribute to the increasing popularity of MIM diodes for several high-frequency applications, such as switching memories [47], hot electron transistors [48], mixers [49], detectors [50,51], and most importantly, as high frequency rectifiers in rectennas for energy harvesting [52-67].

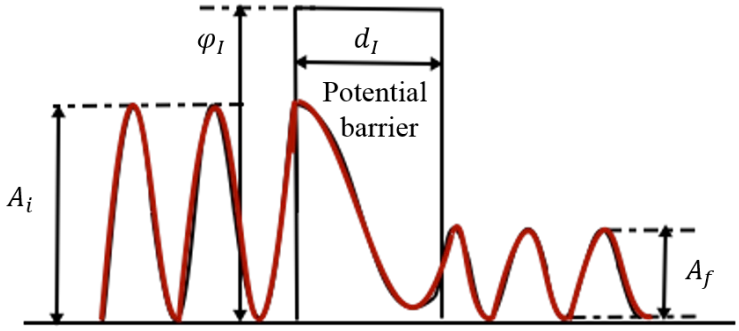

Fig. 2. Schematic of electron tunnelling in MIM diode. Despite a potential barrier (φ_I), with certain thickness (d_I), an incident electron wave function with energy below the barrier can be transmitted through the barrier but the amplitude of the transmitted wave (Ai) is attenuated (Af) [68].

The tunnelling probability increases exponentially with decreasing the barrier thickness, typically <10 nm [69], though recent investigations signalled a thickness below 2 nm [70, 71] to allow the penetration of the tunnelling electrons [72,73].

3.2 CONDUCTION MECHANISMS

The conduction mechanism in MIM diodes relies in their dielectric which electrons are very tightly bonded in it. Dielectric materials are nearly insulators in which the electrical conductivity is very low, and the energy band gap is large. Commonly, the value of energy band gap of insulators is set to be larger than 3 eV or 5 eV. Although not all dielectrics are insulators, all insulators are typical dielectrics [72].

The electric charges in dielectrics will respond to an applied electric field through the change of dielectric polarization. At 0 K, the valence band is filled, and the conduction band is completely empty. Thus, there is no carrier for electrical conduction. But, when temperature is larger than 0 K, there will be some electrons thermally excited from the

valence band and from the donor impurity level to the conduction band. These electrons will contribute to the current transport of the dielectric material.

Similarly, holes will be generated by acceptor impurities and vacancies will be left by excited electrons in the valence band. The conduction current of insulators at normal applied electric field will be very small because their conductivities are inherently low, (i.e., on the order of 10^{-20}~10^{-8} Ω^{-1} cm^{-1}) [73]. However, the conduction current through the dielectric film is noticeable when a relatively large electric field is applied. These noticeable conduction currents are owing to many different conduction mechanisms, which is critical to the applications of the dielectric films.

The classification of conduction mechanisms in dielectric films are main divided in two types the electrode-limited conduction mechanisms or injection-limited conduction mechanisms, and the bulk-limited conduction mechanisms or transport-limited conduction mechanisms. Due to the scope of this work, not all driving mechanisms will be detailed in this work.

The electrode-limited conduction mechanisms include (1) Schottky or thermionic emission (2) Fowler-Nordheim tunnelling, (3) Direct tunnelling, and (4) Thermionic-field emission and are electrical properties associate at the electrode-dielectric contact. While the bulk-limited conduction mechanisms depend only on the properties of the dielectric itself and include (1) Poole-Frenkel emission, (2) hopping conduction, (3) ohmic conduction, (4) space-charge-limited conduction, (5) ionic conduction, and (6) grain-boundary-limited conduction.

The electrode-limited conduction mechanisms depend on the electrical properties at the electrode-dielectric contact and the most important parameters in this type of conduction mechanism are the barrier height at the electrode-dielectric interface and the effective mass of the conduction carriers in dielectric films. The tunnelling current is independent, while thermionic emission mechanism is highly dependent on the temperature.

Aside from the barrier height at the electrode-dielectric interface, is also a key factor in the electrode-limited conduction mechanisms.

3.3 QUANTUM-TUNNELLING

2.3.1 Direct tunnelling

Consider a MIM junction as shown in Fig. 3 Metal 1 (M_1) has a work function (φM_1) lower than the work function (φM_2) of Metal 2 (M_2). In the moment when the two metal electrodes are shorted, tunnelling of electrons occurs from both sides, resulting in the alignment of their Fermi levels (E_F) and when no further flow of electrons takes place, a potential barrier is formed between the electrodes. The barrier height at the metal-insulator interface is determined from the difference between the work function and electron affinity of the insulator, respectively.

The energy band profile exhibits a symmetric barrier when similar metals as electrodes are used (i.e., same work function) as shown in Fig. 3a or an asymmetric band diagram (trapezoidal barrier) with dissimilar metal electrodes [42] as shown in Fig. 3b.

Asymmetric MIM diodes are highly preferred because they do not require external DC bias (zero-bias condition) for producing asymmetric I-V characteristics which, if satisfied, result in the origin of the rectification mechanism in MIM diodes for energy-harvesting applications.

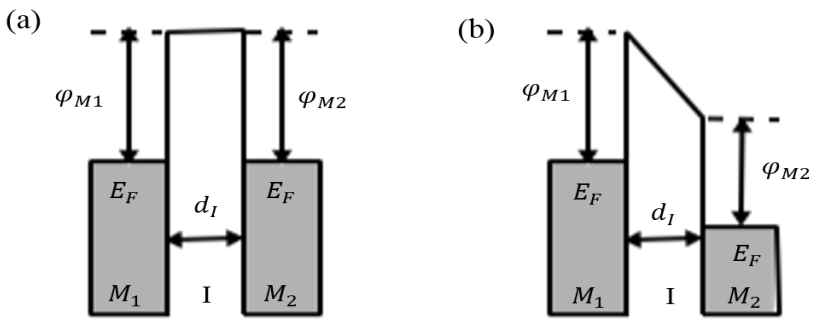

Fig. 3. Energy band diagram in zero-bias condition of (a) symmetric MIM diode, (b) asymmetric MIM diode [42].

2.3.2 Fowler-Nordheim (F-N) tunnelling

According to the classical physics, when the energy of the incident electrons is less than the potential barrier, the electrons will be reflected. However, quantum mechanism predicts that the electron wave function will penetrate through the potential barrier when the barrier is thin enough. Hence, the probability of electrons existing at the other side of the potential barrier is not zero because of the tunnelling effect.

Fig. 4c shows the schematic energy band diagram of Fowler-Nordheim (F-N) tunnelling. F-N tunnelling occurs when the applied electric field is large enough so that the electron wave function may penetrate through the potential barrier into the conduction band of the dielectric.

On applying a bias, the tunnelling probability at one metal-insulator interface becomes larger than that at the other, asymmetricity enhances due to the dissimilarity of barrier heights and the net flow of electrons increases, once the magnitude of biasing voltage becomes larger than the barrier height at the metal-insulator interface, the trapezoidal barrier becomes triangular, resulting in a decrease of tunnelling distance.

In this situation the tunnelling probability exponentially increases, the magnitude of current increases in forward bias, the current in the forward bias condition becomes very large as compared to the equivalent reverse bias, resulting in further enhancement in asymmetry [42].

The expression of the F-N tunnelling [44] current is described in Equation 1:

$$J = \frac{q^3 E^2}{8\pi h q \varphi_B} \exp\left[\frac{-8\pi (2qm_T^*)^{1/2}}{3hE} {\varphi_B}^{3/2}\right] \quad (1)$$

Where:

J is the current density, E is the electric field across the dielectric, h is the Planck's constant, $q\varphi_B$ is the Schottky barrier height (i.e., conduction band offset) and m_T^* is the tunnelling effective mass in dielectric at the absolute temperature (T),

To extract the tunnelling current, the current-voltage (I-V) characteristics are measured at very low temperature to suppress the thermionic emission being tunnelling dominant, for F-N tunnelling a plot of $ln(J/E^2)$ versus $^1/_E$ should be linear.

Biasing of an asymmetric MIM diode at different voltage levels could be used to enhance the asymmetry in applications such as THz mixing, infrared detection, and display technologies [10].

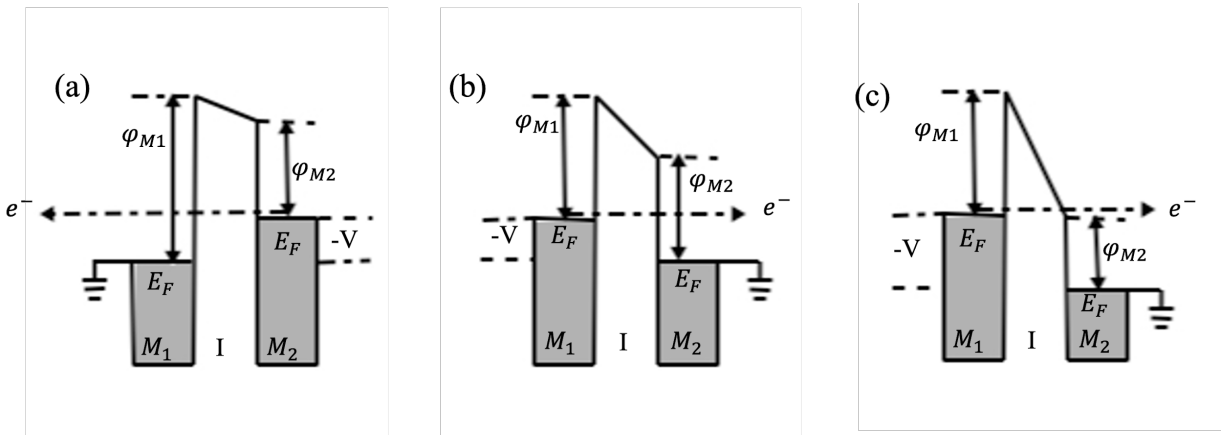

Fig. 4. Energy band diagram of asymmetric MIM diode (a) reverse bias, (b) forward bias, (c) FN tunnelling.

Many factors can decrease the tunnelling probability, the height of the potential barrier formed at the metal-insulator interface. The lower the barrier height, the higher the tunnelling probability. In addition, the magnitude and polarity of biasing voltage also affect the tunnelling probability as they alter the effective barrier height and the tunnelling length [42].

3.4 I-V CHARACTERISTICS

Quantum-tunnelling of electrons was discovered by Esaki in 1957 [74], who described a peculiar p-n junction device which exhibits a decrease in forward current during certain increase in forward voltage and vice versa, this region was defined as negative dynamic resistance (NDR). Later, diodes which exhibit a NDR region, were called tunnel diodes and MIM diodes are a type of tunnel diodes [75]. This NDR region is important due to the possibility to create A.C. power rather than consume it [76].

The NDR region is observed comparing I-V curves of a p-n junction and a tunnel diode as shown in Fig. 5. The three main different features that characterize MIM diodes are: high-asymmetricity, strongly non-linear behaviour (compared to the resistor I-V) which cannot be described using the Ohm's law (i.e., linear resistor behaviour) and the NDR region.

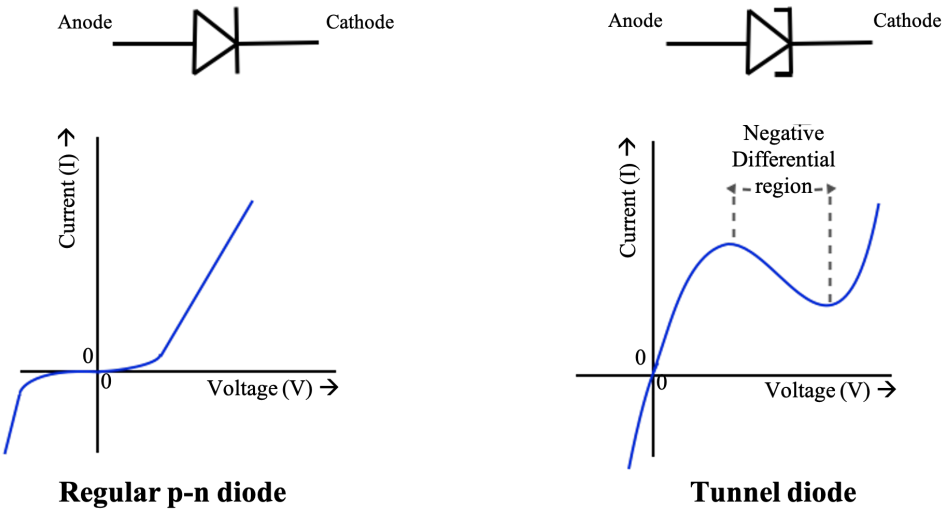

Fig. 5. Current-Voltage (I-V) characteristics of a tunnel diode in comparison with a p-n diode.

The main characteristics of MIM diodes I-V curve can be explained through six main band diagrams as seen in Fig. 6.

At zero bias (no external voltage) there is no current flow (Fig. 6a), when a small forward bias is applied the potential barrier is still very high and there is no noticeable injection and forward current through the junction. However, electrons in the conduction band of the n-region tunnel to the empty states of the valence band in p-region and this creates a forward bias tunnel current (Fig. 6b).

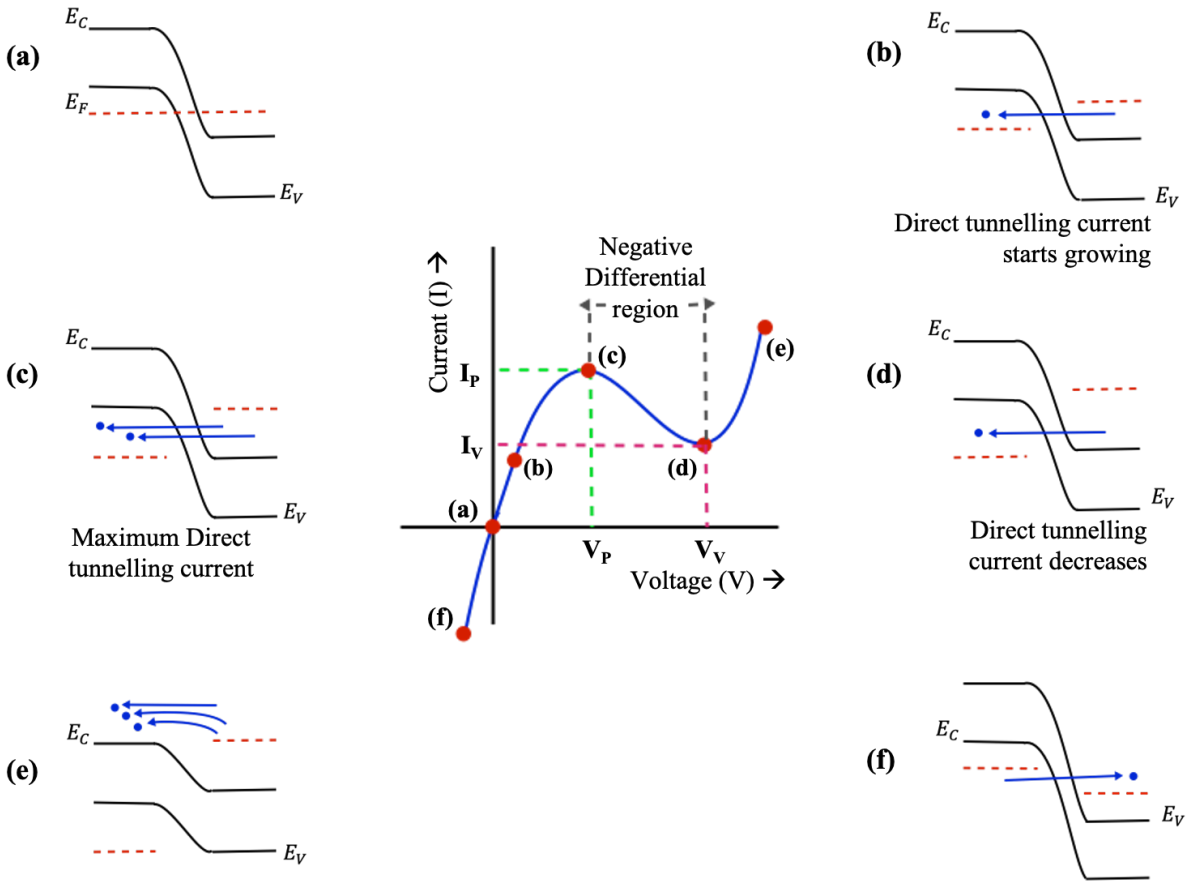

Fig. 6. Typical I-V curve in MIM diodes which outlines six main band diagrams (a) at zero bias (b) initial direct tunnelling, (c) maximum direct tunnelling, (d) tunnelling decay, (e) FN-tunnelling and (f) reverse bias.

At a certain forward voltage (V_p) the energy of the majority of electrons in the n-region is equal to that of the empty states (holes) in the valence band of p-region, this produces a maximum direct tunnelling current (I_p) (Fig. 6c). As the forward bias increases (V_v), the number of electrons in the n-side that are directly opposite to the empty energy states in the valence band decrease and in consequence the tunnelling current decreases (I_v) (Fig. 6d).

When more forward voltage is applied the tunnelling current drops, however the regular diode forward current increases due to electron-hole injection and lower potential barrier. The I-V characteristics further this stage is like a regular p-n diode (Fig. 6e). Under reverse bias, the electrons in the valence band of the p-side tunnel directly towards the empty states present in the conduction band of the n-side creating large tunnelling current which increases with application of reverse voltage (Fig. 6f).

3.5 FIGURES OF MERIT

There are performance metrics required to incorporate diodes for good efficiency as rectifiers for energy harvesting, commonly in IR and optical rectennas [71,77]. The three Figures of merit (FOMs) are asymmetry, non- linearity and responsivity [55]. These characterize the performance of MIM devices however can be equally applied to other diodes.

2.5.1 Asymmetry

Asymmetry describes the diode's ability to perform rectification [42] wherein the electrons flow predominantly in one direction. Mathematically, this is defined as the absolute value of the ratio of forward current to reverse current at a certain bias voltage (Equation 2). A value of 1 indicates full symmetry and hence, no rectification [78,79].

$$f_{ASYM}(V) = \left|\frac{I_F\,(V)}{I_R\,(V)}\right| \tag{2}$$

where I_F is the forward current and I_R is the reverse current.

Asymmetry in MIM diodes is created by using large work function difference metal electrodes and thicker insulator barriers, but this in turn increases the resistance of the diode. Achieving high asymmetry along with low resistance is essential for efficient rectification in the rectenna system [42].

2.5.2 Non-linearity

Non-linearity corresponds to the degree of sharp turn-on voltage [42]. The more non-linear the diode is, the higher the current density at lower voltage. Mathematically, this is defined as the ratio of differential (dynamic) conductance to static conductance [8, 55], and is a measure of the deviation from linear resistor. Non-linearity increases when the insulator thickness decreases [77].

$$f_{NL}(V) = \frac{dI}{dV}\,(V) \quad / \quad \frac{I(V)}{V} \tag{3}$$

where $\frac{dI}{dV}\,(V)$ is the differential conductance and $\frac{I(V)}{V}$ is the static conductance.

2.5.3 Responsivity

Mathematically, responsivity is the ratio of the second derivative of the I-V curve and the differential conductance and is a measure of the rectified signal as a function of input power. High responsivity is required for efficient rectification [42, 79].

$$f_{RES} = \frac{d^2 I}{dV^2}(V) \quad / \quad \frac{dI}{dV}(V) \tag{4}$$

where $\frac{d^2 I}{dV^2}(V)$ is the second derivative of current with respect to the voltage, $\frac{dI}{dV}(V)$ is the differential conductance.

In addition, the three main FOMS there are other equally important criteria for efficient device operation by which the capture wave is transformed to low-frequency power by the diode such are resistance and cut-off frequency [78].

2.5.4 Differential resistance

The diode's differential resistance is obtained by differentiating current on the applied voltage. The lower the resistance of the diode, the higher the current density and the better the impedance matching with a coupling antenna.

$$R_A = 1 \,/\, \frac{d}{dV}(I) \tag{5}$$

where $\frac{d}{dV}(I)$ is the dynamic conductance.

2.5.5 Cut-off frequency

The theoretical model proposed by Sanchez et al. [80] represents the diode as a parallel combination of the nonlinear junction resistance and junction capacitance. Mathematically, it is defined by the following expression,

$$f_C = \frac{1}{2\pi RC} \tag{6}$$

where R is series resistance and C is the capacitance.

The RC (resistance-capacitance) is a governing factor in the rectifier performance, this is the upper limit at which the rectification process is efficient. Above the cut-off frequency rectification is still possible however the strength of the rectified signal at the output of the MIM diode will drop by a factor of approximately $(f_C)^2$, the higher the frequency above f_C the lower the rectification efficiency [59]. To achieve a high cut-off frequency, the RC is constant must be small, which can be obtained with a small junction area [56] and appropriate selection and fabrication.

The cut-off frequency of the whole rectenna device can be evaluated by the following relation,

$$f_C = \frac{R_A + R_D}{2\pi R_A R_D C_D} \quad (7)$$

which considers the antenna impedance $(\mathrm{R_A})$ and the diode resistance $(\mathrm{R_D})$ [64]. R_A is determined by the fabrication process and can be treated as a constant for a given process. The frequency of operation can be increased by keeping a small value of capacitance C_D,

$$C_D = \varepsilon_0 \varepsilon_r \frac{A}{d} \quad (8)$$

where ε_0 is the permittivity of free space, ε_r is the permittivity of insulator material, A is the active area or overlap area of diode and d is the thickness of the insulator layer of diode.

Keeping small values of C_D to increase the frequency operation requires increasing the thickness of the dielectric layer or reducing the contact area. However, the thickness of the insulator layer cannot be increased to promote quantum-tunnelling conduction and increase the non-linearity I-V curve of the MIM diode. The requirement of lower capacitance is attainable only whether the contact area A is minimized.

As an example, for operation of the MIM diode in the optical regime i.e., 650 THz (visible light region), the contact area required is approximately 17 nm x 17 nm [81]. This makes the fabrication of the MIM diode extremely challenging.

3.6 GENERAL CONSIDERATIONS IN FABRICATION

MIM diodes for rectenna applications require advancements in the design, fabrication, and characterisation to enhance its performance and successful implementation for energy harvesting. According to the FOMs mentioned above, the primary limiting factor in the potential performance of a MIM diode is the difference in the work functions of the two metal electrodes. To achieve a high degree of asymmetry in the I-V curve, it is desirable to use metals with highly different work functions. Furthermore, the electron affinity and the dielectric constant are important parameters to choose the ideal materials for the fabrication [79].

Periasamy et al. [13] identified the role of metal electrodes on rectification performance and showed that it is sufficient to choose the metals such that their work function difference is $\Delta\phi\ (\phi M2 - \Delta\phi\ M1)$ is > +30 meV to achieve desired rectification characteristics such as high asymmetry and non-linearity [13]. Ideally, MIM structure should exhibit I-V characteristics with high asymmetry (f_{ASYM} > 1) [61], strong non-linearity (f_{NL} > 3) [71], fast responsivity (f_{RES} > 7 V^{-1}) [66], low hysteresis and low turn-on voltage (close to zero bias) [79]. For impedance matching, Ma and Vandenbosch [65] suggested that the impedance must be of the order of 100 Ω and favour aluminium as being suitable for this application.

The operation in higher frequencies requires greater optimization of the device to address low impedance. The frequency response of the diode is governed by the RC time constant. Since the impedance matching of the antenna and the diode needs to be close, the capacitance needs to be minimized, requiring the minimization of the device area. Also, the geometrical design of the diode is important for rectenna applications [82].

MIM rectifiers, although the most promising rectifier technology, have not been demonstrated at higher frequencies up to 150 THz [58]. Improving MIM fabrication technology and material system design would potentially yield the solution to the rectenna efficiency.

3.7 RECTENNA SYSTEM

The rectenna concept was first demonstrated by Brown et al. in 1964 [56,83], as a highly efficient receiver for microwave power transmission. Nowadays, this concept has been investigated as an energy harvester, mainly solar radiation. Furthermore, the rectenna system has been mentioned by Donchev et al. [71] as an alternative over conventional solar harvesting with photovoltaic (PV) p-n junction solar cells due to its capability to achieve higher efficiencies of energy absorption [73].

The sun as a constant source of energy and its harvesting has been considered as a crucial solution to the ever-increasing demand for clean and renewable energy sources. The rectenna device system operates (Fig. 7) based on the capture and conversion of the energy from an income electromagnetic wave inducing an alternating current (AC) in the conducting antenna and passes the signal at the tuned operating frequency to the rectifier who converts the input AC signal to a usable DC which is transferred to a load [71,78].

The rectenna (RECTifying antENNA) system functions as a receiver and rectifier of the income signal. For this reason, the system is usually designed in the dimensions of the wavelength of the incident wave. Therefore, for microwave frequencies the dimensions are in the scale of centimetres and millimetres (i.e., rectennas) compared with the scale required for infrared (0.3-430 THz) and optical frequencies (430-790 THz) which drop in the micrometres and nanometres units (i.e., nanorectennas). Due to its smaller size, factors such as impedance mismatch and cut-off frequency [58] are the aims of the device's optimization to guarantee the efficient energy absorption.

Goswami et al. [36] highlighted in their work the importance of research into optimized antenna design and fabrication, emphasizing the rectification of the signal as an equally critical issue and a significant challenge [73].

Over the years, new rectifier technologies have emerged replacing the record efficiency achieved with conventional Si Schottky diodes and later with Pt/GaAs Schottky barrier diode (SBD) whose cut-off frequency operation with higher efficiencies

are limited in the GHz frequency and a few THz [46,57,83]. Nowadays, MIM diodes are one of the most promising rectifiers for use in infrared and optical rectennas.

Currently, there is no antenna rectifier device reported to harvest electromagnetic energy at solar frequencies, however there are many publications on rectennas used for optical or IR sensing 52,53,55-67]. The gap between sensing and harvesting lies in the conversion efficiency, defined as the ratio of the output power over the power incident of the antenna, of the incoming signal, being the main limiting factor in the fabrication of a working solar rectenna.

Furthermore, antennas required to receive solar radiation at both visible and infrared regions as need to be design in the nanometre unit [68,84] in comparison with sensing rectennas that are designed in millimetre and micrometre [85] orders of magnitude.

Nanoantennas are promising for receiving solar radiation at both visible and infrared regions as AC electromagnetic signals. Then, the received power is passed to a nanodiode that acts as a rectifier to convert the power from AC to DC form. Nanoarrays are utilized often to increase the captured energy and decrease the number of rectifiers of the entire system. The biggest challenge is how to design an efficient nanoantenna integrate efficiently into a nanodiode to maximize the overall efficiency.

As important criterion for efficient rectenna device operation, Ma and Vandenbosch [63,65] divided the analysis on the efficiency of nanorectennas into two parts – (1) the efficiency by which the light is capture by the antenna and brought to its terminals and (2) the efficiency by which the capture energy is transformed to power by the nanodiode [59,65].

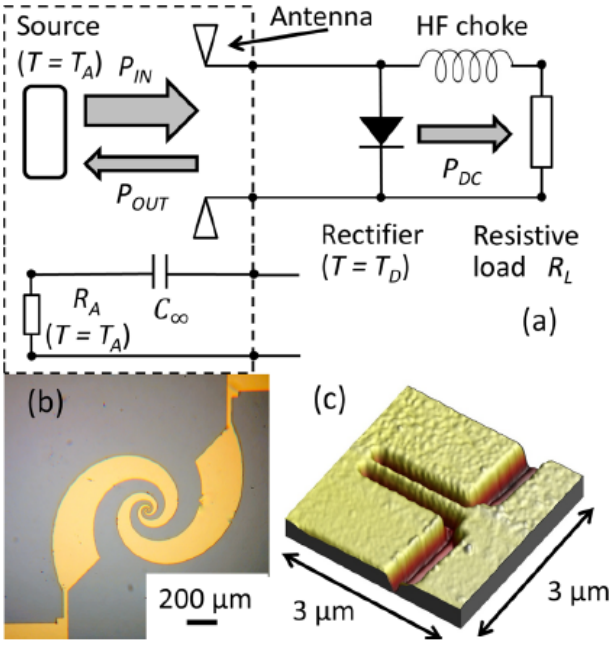

Fig. 7. (a) Schematic of a rectenna. The dashed box shows the equivalent thermal resistor of the antenna illuminated by a source, (b) optical microscope image of the spiral antenna, and (c) atomic force microscope (AFM) image of the self-switching diode [85].

2.7.1 Antenna

Antennas in rectifiers are the receivers or collectors of electromagnetic waves [60]. The energy from a remote source is transferred between them due to the resonance of the antenna which needs to be at least the same wavelength of the incoming signal due this antennas size is designed according the order of magnitude of the wavelength regime. Besides, the classical antenna theory does not apply to nanorectennas at optical frequencies compared to antennas at microwave frequencies.

The precise fabrication of high-frequency antennas to achieve high efficiencies increases the difficulty in manufacturing. Factors such as impedance mismatch in the circuits, parasitic capacitance and inductance, bandwidth direction and polarization of the incidence radiation are necessary to be considered in the antenna design [71].

The dipole antenna is one of the simplest designs, it consists of two identical metals in mirror symmetry, the most common form is two metal rods aligned on the same axis where the length of the metal rod is half the size in the resonant wavelength. However, a variety of designs have been investigated to overcome the narrowband absorption that dipole antennas encounter such as bow-tie antenna [86], spiral [87,88], log-periodic [87,88], microstrip lot [50], and retrodirective rectenna array [60].

2.7.2 Rectifier

A rectifier is a nonlinear device such as a diode which is used as part of the rectenna device to convert an AC input voltage from the antenna into a usable DC voltage. The rectifier limits the rectenna operation by the cut-off frequency of the diode which determines the efficiency of the rectification process. The physical nature of the diode's operation and its potential of achieving a low RC time constant defines changes in the cut-off frequency, therefore, the rectification process.

SBDs have been demonstrated to have high efficiencies limited to frequencies of a few terahertz, whereas MIM diodes are shown to be operational at 150 THz [58, 89] and are predicted to potentially reach the visible regime.

Rectification in these devices is due to variation in tunnelling rates caused by barrier asymmetry due to material selection, device geometry, thermal asymmetry and photoinduced deviation in electron flux distribution across occupied and unoccupied states [90], all contributing toward a nonlinear asymmetric I-V response. The asymmetry comes from the formation of two differential metal-insulator interfaces arising from dissimilar deposition processes, creating regions of enhanced leakage currents through the barrier [71].

Overall, the requirements for the diode are emphasized on low resistance and capacitance, resulting in high cut-off frequency, and high I-V asymmetry at a small bias, implying low leakage and low turn-on voltage.

3.8 FABRICATION TECHNIQUES

Apart from material selection, the fabrication techniques used to manufacture MIM devices are also important for good device performance. The common techniques involved in the deposition of the electrodes are e-beam evaporation, thermal evaporations, and sputtering. Commonly, top and bottom electrodes are patterned using a UV-photolithography technique to improve the efficacy of the diode [26].

The top electrode is the most common point of failure in the fabrication process, the application or contacting of the top conductive electrode could damage the dielectric layer. Also, the use of an organic dielectric layer requires consideration of materials compatibility, metals such as gold (Au), palladium (Pd) and aluminium (Al) are commonly used but there are others, including non-metallic conductive polymers and graphene films [26].

The insulator layer should be uniform in thickness and stoichiometry [79], with low surface roughness and pinhole-free to reduce parasitic capacitance and avoid short-circuiting between electrodes [80]. Ideally, the thickness of the dielectric layer needs to be designed below 2 nm [73], these requirements signalled the most crucial part in MIM diodes fabrication.

To overcome this, self-assembled monolayers (SAMs) have recently been studied as dielectric layer [91], because of their variability in terms of termination chemistry, easy application, consistent thickness (few nanometres) and the ability to tailor metallic properties to improve the charge transport in MIM diode structure [26].

4. METHODOLOGY

The extensive analysis of literature corresponding to processes involved in monolayer formation using self-assembling organic molecules and OTS films, allowed us to identify temperature reaction, maturation time and reaction time (i.e., immersion time) as factors that have an impact in OTS films' quality, defined as uniform and low-thickness OTS monolayers onto the coating substrate.

These two factors, reaction temperature and reaction time, allowed us to design different experiments to know their effects on the quality of the OTS films produced however all the experiments developed followed same 4 steps: i) substrate preparation, ii) OTS/hexane solution preparation, iii) wet coating OTS method, iv) purification and finishing process, with time and temperature variations in steps ii) and iii).

4.1 MATERIALS AND METHODS

The OTS films were produced on 2-inch silicon wafers with a 300 nm thermally grown SiO_2 layer named during experimentation as substrates.

i) The substrate preparation step involved instrumentation and substrates cleaning with piranha solution to remove organic residues that hinder spontaneous ordering process of the OTS molecules for the formation of monolayers. After this, a layer of approximately 25 nm of titanium was deposited by e-beam evaporation. The evaporation system used for the metal deposition was a Moorfield minilab 060 e-beam evaporator (Moorfield Nanotechnology Ltd., Cheshire, UK). The coated substrate was left in the evaporator to avoid contamination while OTs/hexane solution was prepared.

ii) OTS/hexane solution was prepared in the fume cupboard in cleanroom at 20°C and 57% humidity with 0.1 mL of OTS in 50 mL of hexane ($\sim 5 \times 10^{-3}$M

OTS concentration). The hexane was poured in beaker and then OTS was diluted into hexane with an insulin syringe to avoid contact with ambient air. The prepared solution required a maturation time to stabilise chemical components and promote a better monolayer ordering in the OTS films produced. This maturation time varied according the experiment from 5 min, 15 min and 30 min.

iii) Once maturation time was completed, coated substrates were immersed in DIW water and completely dried with N_2 to create a molecular layer of water adsorbed onto substrate surface, according to Britt et al. [17] improves quality of resulting monolayer. Then, coated substrate was immersed in OTS/hexane solution and let it still certain time.

During this step two different experiments were conducted at different temperatures and different reaction times while substrate was immersed into OTS/hexane solution. The temperature experiment required use of temperature controller to set a constant temperature during reaction, and the lack of this equipment in the laboratory make us to design a temperature controller according experiment needs. The reaction times (i.e., immersion time) varied from 30 min, 60 min, 90 min and 120 min and temperatures selected were 0°C, 5°C, 15°C and 20°C.

iv) Once reaction time was achieved some substrates were sonicated at 40 kHz within pure hexane solution during 5 min, others missed this step. Finally, substrates were baked for 15 min at 90°C.

4.2 AFM ANALYSIS

Samples were analysed with atomic force microscopy (AFM) using a Digital Instruments Nanoscope II AFM. All topography images were taken in air under ambient conditions. The AFM measurements were performed in tapping mode using a silicon probe (Tap 300AI-G from Budget Sensors) with the nominal resonance frequency and tip curvature radius of 300 kHz and 8 nm, respectively. Different areas on each sample

were compared to verify that the areas being analysed were typical of the overall surface topography. Analysis and presentation of the AFM data was done using Gwyddion 2.55.

5. RESULTS AND DISCUSSION

The aim of this project was to identify relevant factors during OTS film production that could determine the quality of OTS monolayers with the purpose to design a protocol to be used during MIM diodes fabrication using OTS as dielectric layer. The experimental results were analysed using AFM, however data obtained will require further characterisation techniques to draw firm conclusions.

The AFM analysis of OTS films produced suggest that two relevant factors compromise the uniformity of the monolayers and their manipulation impacts the uniformity in the monolayer described as closely packed molecules and pin-hole free, characteristics required in MIM diodes fabrication.

The relevant aspects are maturation time defined as the resting time that requires OTS/hexane solution once has been prepared, and the reaction temperature during substrate immersion into OTS/hexane solution. Maturation time and reaction temperature are explained in Desbief et. al. [21] as factors that regulate spontaneous ordering processes between OTS molecules that can favour certain alignments into the substrate and thus create uniform monolayers.

In addition, when following what was reported in Etor et al. [5, 6] and Jin et al. [7], it was found that sonication process despite being widely used to remove OTS molecules that were not adsorbed after reaction, can induce loss of uniformity in the monolayer.

The results obtained are organised in 4 sections: monolayer formation, temperature effect on the monolayer, maturation time effect on the monolayer and sonication effect on the monolayer. The top surfaces of the samples (i.e., OTS silanised substrates)

were characterised with AFM technique in tapping mode and sets of height profile images were obtained at different conditions.

5.1 MONOLAYER FORMATION

To a better understanding of OTS films deposited onto silicon substrates was necessary to analyse morphological transitions and roughness differences at proved conditions reported in Jin et al. [7] (20°C, 57% humidity and 60 min immersion time) before varying temperatures and immersion time during wet-chemical OTS coating method.

The samples were imaged after 24 h of preparation and the scanned area was 10 µm x 10 µm, just one sample was scanned at 1 µm x 1 µm due to AFM equipment failure.

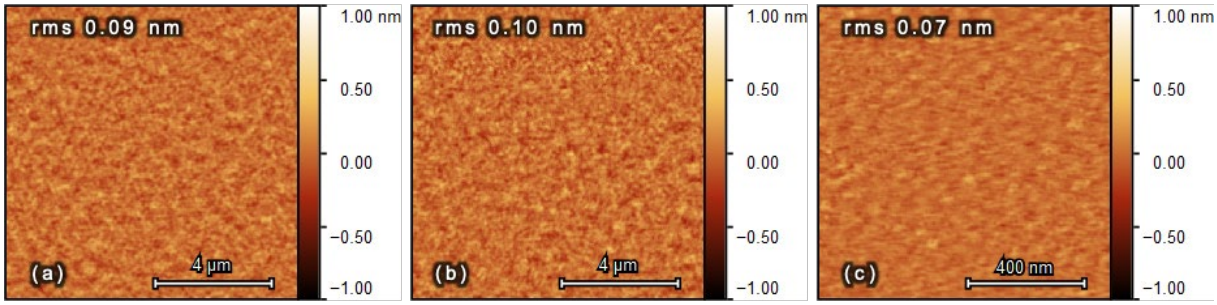

Fig. 14 AFM images of the substrate after: (a) cleaning treatment with piranha solution, (b) 25 nm of titanium deposition, and (c) baking process.

The stages in the OTS film production at clean room conditions were the 4 steps mentioned in the Materials and Methods 4.1 section.

Firstly, the cleaning treatment of the wafers with piranha solution was essential to obtain a uniform and fully grown OTS monolayer at 20°C and after 60 min of substrate immersion. As shown in Fig. 14a clean and smooth native SiO_2 surfaces shown a rms roughness of 0.09 nm (0.9 Å) which is consistent with Lessel et. al. [82] to achieve a smooth and uniform surface. The smaller the rms roughness value, the better the

surface area for its subsequent use in the formation of monolayers and thus, the fabrication of MIM diodes.

However, we found the storage of the substrates, even in cleanroom conditions, increases contamination with grease and other particles that promotes molecule stacking and damages the quality of the monolayer. Thus, to avoid contamination, substrates should be cleaned the same day as OTS-SAMs.

Then, 25 nm of titanium deposition were added with the purpose to simulate OTS conditions in MIM diodes fabrication (Section 5.1). As Fig. 14b shows, the metal deposition slightly increased the rms roughness value to 0.10 nm (1 Å). Further experiments indicated that it did not affect the OTS monolayer smoothness. This suggests it is possible to obtain uniform monolayers between metal electrodes to be used as dielectric layers in MIM diodes.

Finally, Fig. 14c exhibits a fully formed OTS monolayer after an immersion time of 60 min into OTS/hexane solution and 15 min of baking process at 90°C. The quality of the monolayer is evaluated with rms roughness value of 0.07 nm and 2.4 nm of height, these values suggest that it is a potential high-quality monolayer, which is consisted with values reported in Jin et al. [7] and Wang [92] et al.

Overall, Fig. 14c shows homogeneity in the light areas suggesting a more uniform (smooth) surface than the previous steps and their rms values (Fig. 14a and Fig. 14b), this can be explained based on Celestin et al. [26,35], which describes low rms values in monolayers of organic self-assembled molecules due to few variations in the height profile, feature of the molecule used and its carbon chain that remains constant during deposition.

The AFM analysis during the cleaning, titanium deposition and OTS deposition processes allowed us to visualise the topographic profile of each of the steps to be used as a control test for the following experiments in which the temperature and immersion time conditions were varied to observe the changes generated in the monolayer.

For the next stage of the experiments, it was necessary to control temperature during immersion process of substrate in OTS/hexane solution, for this it was necessary to design an equipment capable of generating low temperatures quickly and to maintain temperature constant during the whole process. The design of the temperature controller is described below.

5.2 TEMPERATURE CONTROLLER

To control the temperature during the OTS molecules deposition, it was necessary to design a thermoregulated cooling system that is based on that reported in Brzoska [8] et al. Two main factors were considered in the design, the fast response to reach the target temperature (set point) and the temperature stability during OTS deposition. As show below Fig 13. from bottom to top the system consisted in a water jacket, four thermoelectric peltiers TEC1-12706 model, an upside-down heat sink, two fans of 12 V and a thermal gel jacket. Furthermore, the system was regulated with a STC-1000 temperature controller and four Pt-thermometers which were placed in different zones of the system to analyse heat transfer and to ensure precise temperature control during coating procedure.

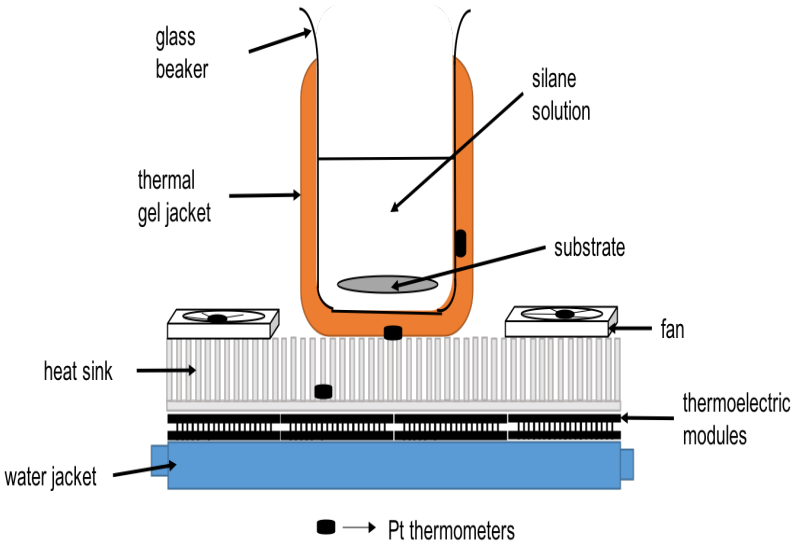

Fig. 13. Schematic of thermo-regulated cooling system.

The thermo-regulated system operated based on peltier modules' effect, peltier's' hot side was attached to a water jacket where cold water removed heat from the device while peltier's cool side was attached to an inverted heat sink which in this position allowed to easily spread cooling effect through heat sink fins. The heat sink fins provided large surface area for the air to pass through and be cooled quickly and fans cooled thermal-gel jacket by heat transfer convection. The system created achieved to decrease glass beaker temperature and consequently temperature of the solution.

5.2.1 Temperature controller constraints

The temperature controller was accurate enough to cool during OTS deposition process however, it had some limitations. First, the controller installed was an ON/OFF system with cycles of one minute, due to this at each cycle, fans and peltier's modules were turned on/off to increase or decrease temperature of the thermal gel jacket and beaker. However, the one-minute cycle was so long that it induced huge variation in the reaction's temperature. For future experiments, it is recommended to use a controller with shorter cycles so the user can maintain constant the temperature without considerable fluctuations.

The second limitation of this cooling system was the contamination of the solution by ambient humidity. When the humid air reached temperatures below 10°C, water droplets condensed on the surface of the beaker and rolled into the solution, causing destabilisation of the OTS cross-linking described in step 4 "In-plane reticulation" in section 2.3 Fig. 9 and thus, leading to undesirable stacking of OTS molecules on the substrate. To avoid this type of contamination in future experiments we suggest using a humidity chamber during OTS deposition to avoid water condensation.

Due to these limitations, it was impossible to continue with experimentation at low temperatures without causing irregular OTS deposition on substrate. The next section shows our findings at low temperatures however, it requires further investigation with updates in temperature controller which does not allow for firm conclusions.

5.3 Temperature effect on monolayer

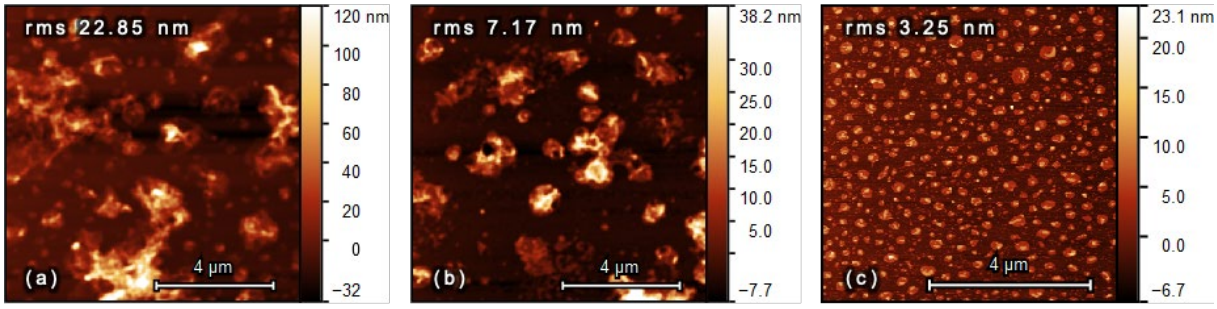

Fig. 15. AFM images (10 µm x 10 µm) signalling OTS crosslinking effect at low temperatures (a) 10°C, (b) 5°C, and (c) 0°C after 60 min of immersion.

The results obtained by lowering the temperature during OTS molecules deposition were not as expected, since, due to the nature of the equipment designed to keep temperature constant, it was difficult to avoid water condensation and contact with the OTS/hexane solution. However, the images shown in Fig. 15 are consistent with existing models that explain how self-assembled molecules are ordered to subsequently attach to the substrate.

The set of AFM images shown in Fig. 15 were obtained during the OTS deposition process at 10°C, 5°C and 0°C respectively, and all show the cross-linking effect. The presence of moisture condensation in OTS solution affected the reticulation process causing overlapping of OTS monolayer segments at nucleation or anchoring points on substrate, this is visualised by observing the height range of images and their rms roughness values being extremely high compared to that reported for a full OTS monolayer obtained at 20°C that is 2.4 nm height and rms roughness 0.07 nm according to Jin et al. [7] and Wang [92] et al.

However, the interest in these images is that they are visually consistent with the two main models that explain the process which self-assembling molecules attach to the substrate, these being the "island aggregation" and "uniform aggregation" models.

The presence of large dendritic-shaped aggregates or "islands" (Fig. 15a) agrees with the reported growth mechanism in several investigations [17,8,9,11,17,33], which

starts with building of dispersed islands in solution that adhere to substrate and grow together to form a complete monolayer. Similarly, Fig. 15b differs by having less connected and more compact "islands", which is consistent with that reported in Kellner et al. [9] that explains this aggregation change due to the loss of diffusion generated by using low temperatures.

Fig. 15c does not follow the "island aggregation" model as it shows different molecular arrangement describes as compact clusters with similar dimensions and fully distributed on the substrate. This molecular distribution is consistent with that is described by Wasserman et al. [93] who support the "uniform aggregation" model as a homogeneous molecular distribution on the substrate in a disordered manner that subsequently fills and reorganises into the final monolayer.

From this, we can suggest that to promote a fully formed OTS monolayer in a short period of time defined as less than 60 min, it is necessary to maintain temperature between 10°C-20°C. We cannot set a more defined temperature value as further investigation is needed without generating cross-linking between the molecules, however, this range of temperature is consistent with findings of Carraro et al. [10] and Desbief et al. [11].

In summary, Fig. 15 shows that low temperatures defined at less than 20°C affect the formation of the OTS monolayer and the obtention of high-quality monolayer describe as well ordered and tightly packed. It is essential to keep the reaction temperature between a range of 10°C to 20°C, as lower temperatures reduce natural movement of the molecules which is consistent with Kellner et al. [9], at low temperatures, kinetics effect dominates over thermodynamics compromising the diffusion of molecules and this creates compact and round shapes.

5.4 MATURATION TIME EFFECT ON MONOLAYER

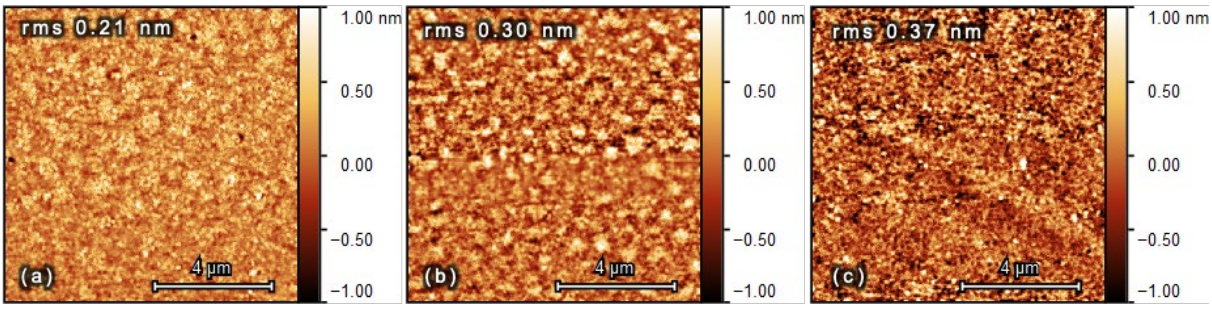

Fig. 16. AFM images (10 µm x 10 µm) illustrate the effect of "maturation time" or OTS solution rest time of (a) 30 min, (b) 15 min and (c) 5 min prior to substrate immersion.

Our findings suggested that OTS/hexane solution maturation prior wafer immersion was essential to obtain well-ordered and closely packed OTS monolayers. Desbief et al. [11], Lambert et al. [32] and Foisner et al. [34] have signalled that a pre-organisation of molecules exists in the solution which increases the monolayer growth rate. This maturation time is described as the time between molecule solubilisation, and the beginning of the silanisation reactions once substrate added into OTS/hexane solvent. This phenomenon promotes better island formation and surface coverage, which means better monolayer quality [8].

The AFM images analysis of the films produced in Fig. 16 a), b) and c) illustrate the different molecular arrangement to form a single monolayer at 20°C and 60 min of substrate immersion, findings suggest that decreasing the OTS/hexane maturation time brings loss on the molecular compaction which is consistent with data reported in Kojio et al. [33] and Aswal et al. [14,15]. The OTS monolayer obtained presented more gaps (i.e., darker areas) and less uniformity when the maturation time of the solution decreased.

Fig. 16a illustrates the final high-quality OTS monolayer obtained at 20°C, 30 min of OTS/hexane maturation time and 60 min of reaction (i.e., substrate immersion), and it had a rms roughness of 0.21 nm and a thickness of 2.8 nm.

Fig. 16b and 16c are explained according to Kojio et al. [33] and Aswal et al. [14,15] that signalled the growth mechanism of crystalline OTS monolayers and reported a hexagonal molecular arrangement during the OTS-SAM formation.

During maturation time isolated and closely packed OTS molecules islands are formed in solution, and these islands then during substrate immersion serve as aggregation centres for molecules diffusing on the surface as well as for adsorbing from solution. At low surface coverage, the fractal dimension of the islands increases with surface coverage, and at higher surface coverage islands grow by branching and eventually coalesce. Finally, the inter-island regions (pores and pinholes) shrink and eventually form a continuous monolayer.

Our results suggested that to promote high-quality OTS monolayers is important to consider a maturation time of the OTS/solvent solution of at least 30 min

5.5 SONICATION EFFECT ON MONOLAYER

Findings about sonication effects on OTS monolayers are part of the fourth step “Purification and Finishing” signalled in Materials and Methods section 4.1, according to Jin et. al [7] part of the coating process in MIM diodes fabrication with OTS monolayers is the sonication of the substrate after being removed from the OTS/ hexane solution with the purpose to remove non-deposited OTS molecules. However, the AFM analysis of the films produced following this step suggest that sonication induced molecular stacking and loss of the monolayer which is consistent with data reported in Brzoska et. al [8].

At molecular level, the newly formed bonds that build the monolayer require first the removal of water to stabilise the covalent bonds between the substrate and the monolayer, which is why when vibrations are induced by sonication many of these bonds are lost and consequently agglomerates of molecules are generated.

Figure 17. shows AFM images taken on OTS-coated substrates with and without the sonication step. In addition, it was evaluated whether increasing the immersion time of the substrate in the OTS solution could further stabilise the monolayer by avoiding agglomeration of molecules. The images are set in 2 columns x 3 rows to an easy comparison between them, rows indicate substrates without and with sonication respectively and columns indicate different immersion times, 60 min, 90 min and 120 min respectively.

The images in the second column exhibit brighter and bigger circled areas than first column, this can be explained with reported in Britt et al. [16] as molecule stacking, suggesting that the use of sonication post OTS deposition is not recommended, as it does not allow a settlement time of the newly formed monolayer which after the baking process will firmly anchor to the substrate.

Because of this, we suggest avoiding the sonication process once the substrate has been removed from the OTS solution and to continue with the substrate annealing process.

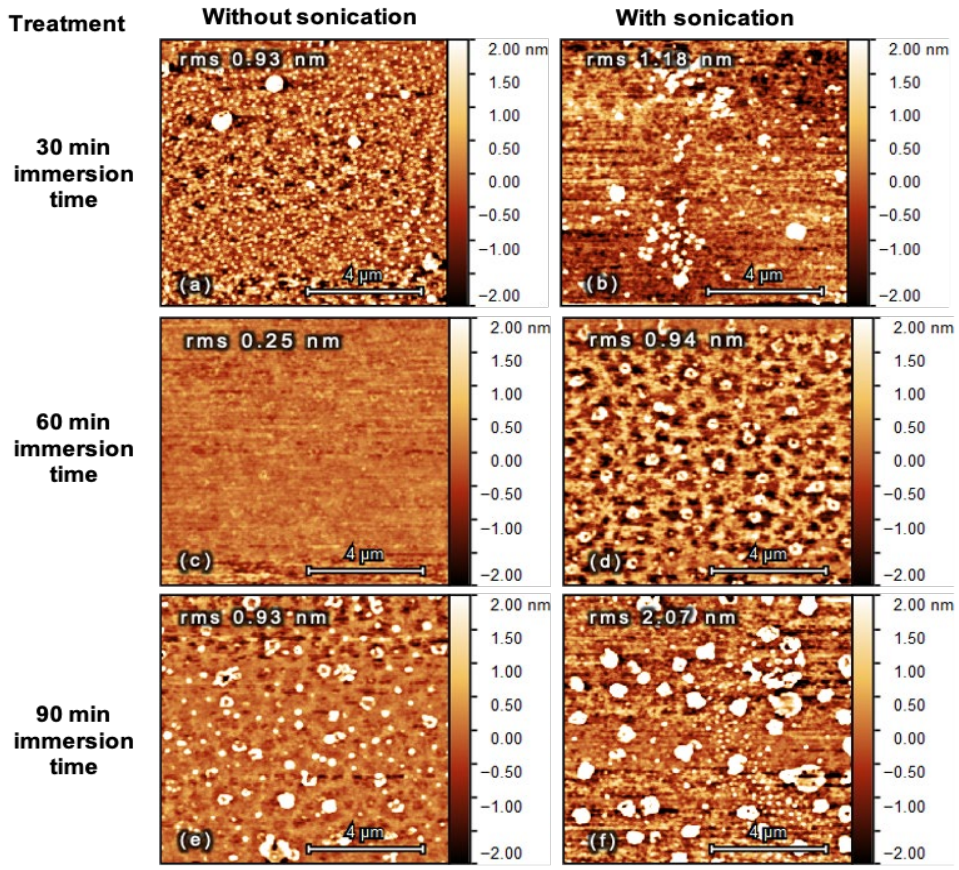

Fig. 17. AFM images (10 µm x 10 µm) illustrate the effect of sonication in the OTS solution prior to substrate immersion. Images a) and b) are samples obtained at 60 min substrate immersion without and with sonication, respectively. Images c) and d) are samples obtained at 90 min substrate immersion without and with sonication, respectively. Images e) and f) are obtained after 120 min substrate immersion, without and with sonication, respectively.

On the other hand, from this experimentation we could notice that even without the sonication step, stacking of molecules can be generated by increasing the immersion time of the substrate in the solution, being the ideal time of 60 min in which the substrate should be left to rest in the solution without external disturbances or sonication process.

5.6 PROTOCOL TO OTS DEPOSITION

The main purpose of this project was to emphasise temperature and time conditions during OTS coating in MIM diodes fabrication as relevant factors that can induce better performance as dielectric layer. Although further analysis of the OTS films produced is required, a protocol was developed to use OTS films in MIM diodes fabrication.

The developed protocol takes as a reference Jin et al. MIM diodes fabrication [3] to focus just on the process involving OTS coating on 300 nm SiO_2 substrates previously coated with 25 nm titanium exemplified in Fig. 12e.

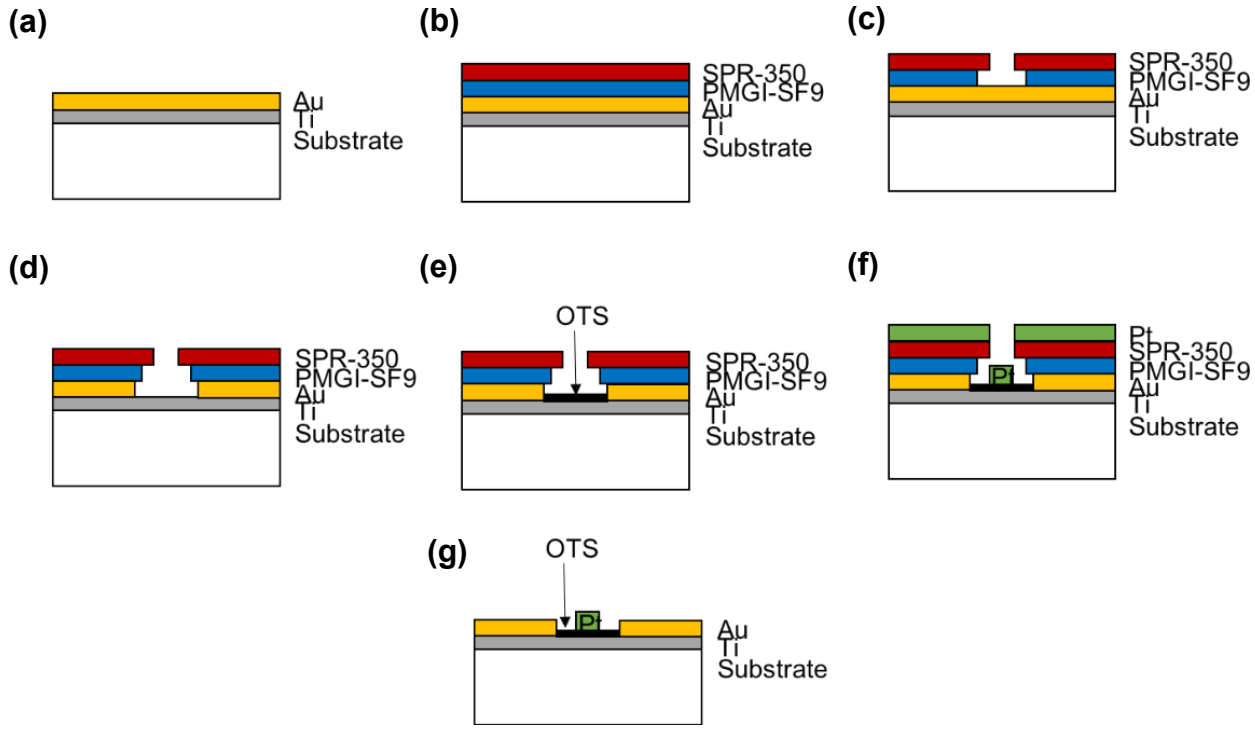

Fig. 12. Schematic of MIM diode fabrication based on Jin et al. [7].

5.6.1 Preparation

Wet-chemical processing was used as a method for OTS deposition in which adsorption, self-assembly and covalent bonding attach the molecules onto the silicon oxide wafer.

Following Brzoska et al. [8] and Lessel et al. [21] procedure, the process consisted of four basic steps which will be detailed in the following sections.

i. Instrumentation cleaning, such as beakers and tweezers
ii. Wafer cleaning
iii. Preparation of the OTS/solvent solution
iv. Coating procedure

5.6.1.1 Instrumentation cleaning

The cleaning procedure requires the preparation of a piranha solution consisting of 75% sulphuric acid (H_2SO_4) and 25% hydrogen peroxide (H_2O_2). Once piranha solution is prepared, placed tweezers inside beakers of 500 mL, filled beakers with piranha solution, tilt and slowly rotate so the solution can reach the bezel of the beaker. After 20 min rinse beakers and tweezers 10 times in deionized water (DIW). Repeat the procedure twice, each with fresh piranha solution and fresh DIW. Finally, dry beakers and tweezers with Nitrogen (N_2) and store in a clean environment.

5.6.1.2 Solution preparation

Prepare an OTS/Hexane solution with 0.1 mL of OTS in 50 mL of hexane ($\sim 5 \times 10^{-3}$ M OTS concentration) in a beaker. Firstly, pour hexane solvent in the beaker, then using a vacuum chamber take 0.1 mL of OTS with an insulin syringe, after this procedure dilute OTS into hexane releasing small droplets of OTS avoiding creating bubbles that can induce air to the solution. Let the solution still 30 min. The appearance of white flakes or filaments indicates an uncontrolled cross-linking of silane molecules caused by contact of the solution with water of humid air and in this case the solution needs to be replaced.

5.6.2 Coating procedure

For this procedure wafer need to be previous coated with titanium and gold according steps a) to d) in Fig 12. The reaction temperature needs to be controlled and keep constant for 60 min (vacuum chamber is suggested).

First, take clean substrate out from the breaker with DIW and dry completely with N_2, then leave in the ambient clean-room humidity (57%) for 5 min. Afterwards, put wafer into the OTS/ hexane solution during 60 min while monitoring temperature maintain constant. After this, there is no need for controlling temperature, take wafer out and flushes it with pure hexane to remove unbound silane molecules. Finally, bake wafer for 15 min at 90°C to complete OTS monolayer assembly and to remove any residual solvent.

Finally, proceed with steps f) and g) shown in Fig 12. To complete MIM diodes fabrication.

6. CONCLUSIONS

This present work addressed how to grow OTS monolayers with high uniformity and low thickness to further on, use them as dielectric layers in MIM diodes. Most of the objectives were accomplished, the acknowledgement of the insulator layer and its requirements in the MIM diode fabrication process and the identification of the relevant conditions in the monolayer growth to promote uniformity and pinhole-free layers. Our hypothesis was partially proven, the differences in the OTS monolayer are attributed to the variation in the reaction conditions. However, further investigation is necessary to evaluate the OTS monolayers performance as dielectric in MIM diodes fabrication.

Collectively, the evidence we have presented tells that to promote a uniform OTS monolayer growth, the main aspects needed to obtain high-quality and reproducible OTS monolayers are maturation time and a low temperature of reaction (below 20°C). The maturation time allows a pre-organisation of molecules in the OTS solution which increases the monolayer growth rate, promotes a better “island” aggregation and surface coverage, which means better monolayer quality.

Moreover, the reaction temperature has an impact on the fashion molecules aggregates in the monolayer. At temperatures near to 20°C, the monolayer requires around one hour to be fully formed, while at temperatures between 20°C-10°C require more time, and the possibility of water condensation is high. At low temperatures (below 10°C), the solution is easily exposed to air humidity increasing the risk of crosslinking. The use of low temperatures in the monolayer formation requires additional investigation and improvements in the thermo-regulated system to keep temperatures constant during longer times.

Furthermore, our results indicate that an accurate recipe for high-quality monolayer growth requires an OTS concentration of 5×10^{-3} M, with an OTS/hexane solution maturation time of 30 min, and a reaction time (i.e., substrate immersion in the solution) of 60 min, with an OTS solution temperature from 10°C to 20°C, and without a final sonication before baking process.

However, further experiments should be conducted to evaluate their electrical properties and their long-term stability. First, we can evaluate the electrical properties of the monolayers using a J-V curve. For example, we can compare the performance of ordered and disordered monolayers (as the ones obtained with the sonication step) plotting their current density as a function of voltage. Since ordered monolayers are time-consuming and more costly to produce, the plots would tell us which monolayer has the best performance subject to their production costs. Also, with this method we can also test their electrical properties through time comparing their performance after preparation and upon aging.

Therefore, additional investigation is needed to know the long-term stability of the monolayers. For this purpose, we can analyse the gradual oxidation of the molecules with XPS measurements in the carbon and oxygen peaks. While an increase in the oxygen peak through time represents the sample aging, a decrease in carbon means its degradation. Therefore, to measure these peaks after preparation and during time, we can estimate its useful life and its possible effect on MIM diodes.

Finally, to create better MIM diodes we require to understand the charge-transport mechanism variation and the ability to control the oxidation on monolayers. Although MIM diodes were not fabricated in this work, its fabrication is necessary to evaluate the monolayer behaviour as dielectric and to test its interaction with the metal electrodes.

7. REFERENCES

1. 1. Carter F., Siatkowski R., and Wohltjen H., *A pioneer in molecular electronics*. Biosensors and Biocomputers. 1989, Boston, MA: Springer. 454.
2. Sabatani E. and Rubinstein I., *Organized Self-Assembling Monolayers on Electrodes. 2. Monolayer-Based Ultramicroelectrodes for the Study of Very Rapid Electrode Kinetics.* The Journal of Physical Chemistry, 1987: p. 6663-6669.
3. Finklea H., *Self-Assembled Monolayers on Electrodes.,* in *Encyclopedia of Analytical Chemistry*. 2006, Wiley Online Library.
4. Krzeminski C., et al., *Theory of electrical rectification in a molecular monolayer.* Physical Review B, 2001. **64**(8).
5. Etor D., et al., *An Ultrathin Organic Insulator for Metal–Insulator–Metal Diodes.* IEEE Transactions on Electron Devices, 2016. **63**(7): p. 2887-2891.
6. Etor D., *Optimising the Structure of Metal-Insulator-Metal Diodes for Rectenna Applications*, in *Durham theses*. 2016, Durham University: Durham, UK.
7. Jin J., et al., *Metal-insulator-metal diodes based on alkyltrichlorosilane self-assembled monolayers.* AIP Advances, 2019. **9**(6): p. 1-6.
8. Brzoska J., Azouz B., and Rondelez F., *Silanization of solid substrates: A step toward reproduciblity.* American Chemical Society, 1994. **10**: p. 4367-4373.
9. Kellner B., Muller-Landau F., and Cadenhead D., *The Temperature-Dependence Characterization of Insoluble Films at the Air-Water Interface.* Journal of Colloid Science, 1978. **66**(3).
10. Carraro C., et al., *Observation of Three Growth Mechanisms in Self-Assembled Monolayers.* The Journal of Physical Chemistry B, 1998. **102**(23): p. 4441-4445.
11. Desbief S., et al., *Impact of chain length, temperature, and humidity on the growth of long alkyltrichlorosilane self-assembled monolayers.* PCCP, 2011. **13**(7): p. 2870-2879.
12. Cowell E. W. 3rd., et al., *Advancing MIM electronics: amorphous metal electrodes.* Advanced Materials, 2011. **23**(1): p. 74-78.
13. Periasamy P., et al., *Metal-insulator-metal diodes: role of the insulator layer on the rectification performance.* Advanced Materials, 2013. **25**(9): p. 1301-1308.
14. Aswal D. K., et al., *Self assembled monolayers on silicon for molecular electronics.* Analytica Chimica Acta, 2006. **568**(1–2): p. 84-108.
15. Aswal D. K., et al., *A Tunnel Current in Self-Assembled Monolayers of 3-Mercaptopropyltrimethoxysilane.* Small, 2005. **1**(7): p. 725-729.
16. Britt, D. and Hlady V., *An AFM Study of the Effects of Silanization Temperature, Hydration, and Annealing on the Nucleation and Aggregation of Condensed OTS Domains on Mica.* Journal of Colloid and Interface Science, 1996. **178**(2): p. 775-784.
17. Wang Z., et al., *The Porter-Whitesides Discrepancy: Revisiting Odd-Even Effects in Wetting Properties of n-Alkanethiolate SAMs.* Coatings, 2015. **5**(4): p. 1034-1055.
18. Ulman A., *An Introduction to Ultrathin Organic Films*. Academic Press. Vol. 4(4). 1991, Boston. 442.
19. Bigelow W. C., Pickett D. L., and Zisman W. A., *Oleophobic monolayers: I. Films adsorbed from solution in non-polar liquids.* Journal of Colloid Science, 1946. **1**(6): p. 513-538.
20. Maoz R. and Sagiv J., *On the formation and structure of self-assembling monolayers. I. A comparative atr-wettability study of Langmuir - Blodgett and adsorbed films on flat substrates and glass microbeads.* Journal of Colloid and Interface Science, 1984. **100**(2): p. 465-496.
21. Lessel M., et al., *Self-assembled silane monolayers: an efficient step-by-step recipe for high-quality, low energy surfaces.* Surface and Interface Analysis, 2015. **47**(5): p. 557-564.
22. Kumar V., et al., *Self assembled monolayers of octadecyltrichlorosilane for dielectric materials*, in *AIP Conference Proceedings*. 2016.

23. Dong J., et al., *Self-assembly of octadecyltrichlorosilane monolayers on silicon-based substrates by chemical vapor deposition.* Thin Solid Films, 2006. **515**(4): p. 2116-2122.
24. Jung M-H. and Choi H-S., *Characterization of octadecyltrichlorosilane self-assembled monolayers on silicon (100) surface.* Korean Journal of Chemical Engineering, 2010. **26**(6): p. 1778-1784.
25. Katz E., Shipway A. N., and Willner I., *7 - Electronic and Optical Transduction of Photoisomerization Processes at Molecular- and Biomolecular-Functionalized Surfaces.* Photoreactive Organic Thin Films, Academic Press, 2002: p. 219-268.
26. Celestin M., et al., *A review of self-assembled monolayers as potential terahertz frequency tunnel diodes.* Nano Research, 2014. **7**(5): p. 589-625.
27. Dannenberger O., Buck M., and Grunze M., *Self-Assembly ofn-Alkanethiols: A Kinetic Study by Second Harmonic Generation.* The Journal of Physical Chemistry B, 1999. **103**(12): p. 2202-2213.
28. Rozlosnik N., Gerstenberg M., and Larsen N., *Effect of Solvents and Concentration on the Formation of a Self-Assembled Monolayer of Octadecylsiloxane on Silicon (001).* Langmuir, 2003. **19**: p. 1182-1188.
29. Bain C. D., et al., *Formation of Monolayer Films by the Spontaneous Assembly of Organic Thiols from Solution onto Gold.* American Chemical Society, 1989. **111**: p. 321-335.
30. Thomas R. C., et al., *Real-time measurements of the gas-phase adsorption of n-alkylthiol mono- and multilayers on gold.* Langmuir, 1991. **7**(4): p. 620-622.
31. Silberzan P., et al., *Silanation of silica surfaces. A new method of constructing pure or mixed monolayers.* Langmuir, 1991. **7**(8): p. 1647-1651.
32. Lambert A., et al., *A Protocol for the Reproducible Silanization of Mica Validated by Sum Frequency Spectroscopy and Atomic Force Microscopy.* American Chemical Society, 2000. **16**(22): p. 8377-8382.
33. Kojio K., et al., *Molecular Aggregation State of n-Octadecyltrichlorosilane Monolayers Prepared by the Langmuir and Chemisorption Methods.* Langmuir, 2000. **16**(8): p. 3932-3936.
34. Foisner J., et al., *Atomic Force Microscopy Investigation of the Growth of Different Alkylsiloxane Monolayers from Highly Concentrated Solutions.* Langmuir, 2003. **19**(9): p. 3741-3746.
35. Celestin M., et al., *Tunnel Diodes Fabricated For Rectenna Applications Using Self-Assembled Nanodielectrics.* Procedia Engineering, 2010. **5**: p. 1055-1058.
36. Goswami D. Y., et al., *New and emerging developments in solar energy*. Solar Energy, 2004. **76**(1-3): p. 33-43.
37. Parikh A., et al., *An Intrinsic Relationship between Molecular Structure in Self-Assembled n-Alkylsiloxane Monolayers and Deposition Temperature.* The Journal of Physical Chemistry A, 1994. **98**(31): p. 7577-7590.
38. Bierbaum K., et al., *Growth of Self-Assembled n-Alkyltrichlorosilane Films on Si(100) Investigated by Atomic Force Microscopy.* Langmuir, 1995. **11**(6): p. 2143-2150.
39. Zangmeister C. D., et al., *Energy-level alignment and work function shifts for thiol-bound monolayers of conjugated molecules self-assembled on Ag, Cu, Au, and Pt.* Chemical Physics Letters, 2007. **442**(4-6): p. 390-393.
40. Azad I., et al., *Design and fabrication of metal-insulator-metal diode for high frequency applications*, in *Infrared Technology and Applications XLIII*. 2017.
41. Ratnadurai R., et al., *Nanomanufacturability Of Thin Film MIM Diodes.* AIP Conference Proceedings, 2010. **1313**(1): p. 403-405.
42. Shriwastava S. and Tripathi C., *Metal-Insulator-Metal Diodes: A Potential High Frequency Rectifier for Rectenna Application.* Journal of Electronic Materials, 2019. **48**(5): p. 2635-2652.
43. Fisher J. C. and Giaever I., *Tunneling Through Thin Insulating Layers.* Journal of Applied Physics, 1961. **32**(2): p. 172-177.

44. Simmons J. G., *Conduction in thin dielectric films.* Journal of Physics D: Applied Physics, 1971. **4**(5): p. 613-657.
45. Champlin K. S. and Eisenstein G., *Cutoff Frequency of Submillimeter Schottky-Barrier Diodes.* IEEE Transactions on Microwave Theory and Techniques, 1978. **26**(1): p. 31-34.
46. Giovine E., et al., *Fabrication of Schottky diodes for terahertz imaging.* Microelectronic Engineering, 2011. **88**(8): p. 2544-2546.
47. Waser R. and Aono M., *Nanoionics-based resistive switching memories.* Nature Materials, 2007: p. 833–840.
48. Heiblum M., *Tunneling hot electron transfer amplifiers (theta): Amplifiers operating up to the infrared.* Solid-State Electronics, 1981. **24**(4): p. 343-366.
49. Masalmeh S. K., Stadermann H. K., and Korving J., *Mixing and rectification properties of MIM diodes.* Physica B: Condensed Matter, 1996. **218**(1-4): p. 56-59.
50. Krishnan, S., et al., *Design and development of batch fabricatable metal–insulator–metal diode and microstrip slot antenna as rectenna elements.* Sensors and Actuators A: Physical, 2008. **142**(1): p. 40-47.
51. Krishnan S., et al., *Thin Film Metal-Insulator-Metal Junction for Millimeter Wave Detection.* Procedia Chemistry, 2009. **1**(1): p. 409-412.
52. Aldrigo M., et al., *Design rules for innovative nano-rectennas in the infrared region.* 2013 European Microwave Conference, 2013.
53. Gadalla M. N., Abdel-Rahman M., and Shamim A., *Design, optimization and fabrication of a 28.3 THz nano-rectenna for infrared detection and rectification.* Scientific Reports, 2014. **4**(4270): p. 1-9.
54. Khan A. A., et al., *Metal-insulator-metal diodes with sub-nanometre surface roughness for energy-harvesting applications.* Microelectronic Engineering, 2017. **181**: p. 34-42.
55. Gustafson T. K., Schmidt R. V., and Perucca J. R., *Optical detection in thin-film metal-oxide-metal diodes.* Applied Physics Letters, 1974. **24**(12): p. 620-622.
56. Brown W. C., *Optimization of the Efficiency and Other Properties of the Rectenna Element*, in *IEEE-MTT-S International Microwave Symposium*. 1976 Cherry Hill, NJ, USA. p. 142-144.
57. McSpadden J. O., Yoo T., and Chang K., *Theoretical and Experimental Investigation of a Rectenna Element for Microwave Power Transmission.* IEEE Transactions on Microwave Theory and Techniques, 1992. **40**(12): p. 2359-2366.
58. Berland B., *Photovoltaic Technologies Beyond the Horizon: Optical Rectenna Solar Cell*, U.S.D.o.E. Laboratory, Editor. 2003, National Renewable Energy Laboratory. p. 1-21.
59. Sarehraz M., et al., *Rectenna Developments for Solar Energy Collection*, in *Record of the Thirty-first IEEE Photovoltaic Specialists Conference*. 2005: Lake Buena Vista, FL, USA. p. 78-81.
60. Ren Y-J. and Chang K., *New 5.8-GHz circularly polarized retrodirective rectenna arrays for wireless power transmission.* IEEE Transactions on Microwave Theory and Techniques, 2006. **54**(7): p. 2970-2976.
61. Chiou H-K. and Chen i-S., *High-Efficiency Dual-Band On-Chip Rectenna for 35- and 94-GHz Wireless Power Transmission in 0.13-μm CMOS Technology.* IEEE Transactions on Microwave Theory and Techniques, 2010. **58**(12): p. 3598-3606.
62. Bareiß M., et al., *Nano-transfer printing of functioning MIM tunnel diodes*, in *IEEE Silicon Nanoelectronics Workshop*. 2012: Honolulu, HI. p. 1-2.
63. Vandenbosch G. and Ma Z., *Upper bounds for the solar energy harvesting efficiency of nano-antennas.* Nano Energy, 2012. **1**(3): p. 494-502.
64. Briones E., Alda J., and Gonzalez F. J., *Conversion efficiency of broad-band rectennas for solar energy harvesting applications.* Optics Express, 2013. **21**: p. A412-8.
65. Ma Z. and Vandenbosch G., *Optimal solar energy harvesting efficiency of nano-rectenna systems.* Solar Energy, 2013. **88**: p. 163-174.
66. Moddel G. *Will Rectenna Solar Cells Be Practical?* in *Rectenna Solar Cells*. 2013. Berlin, Germany: Springer.

67. Etor D., et al., *High-frequency metal-insulator-metal (MIM) diodes for thermal radiation harvesting*, in *2015 40th International Conference on Infrared, Millimeter, and Terahertz waves (IRMMW-THz)*. 2015. p. 1-2.
68. Kotter D. K., et al., *Theory and Manufacturing Processes of Solar Nanoantenna Electromagnetic Collectors.* Journal of Solar Energy Engineering, 2010. **132**(011014): p. 1-9.
69. Eliasson B. J., *Metal-Insulator-Metal Diodes For Solar Energy Conversion*, in *Department of Electrical and Computer Engineering*. 2001, University of Colorado: Boulder, Colorado, US. p. 217.
70. Silva L. L., Rosa-Almeida V., and Dos Santos N. A., *Metal-Insulator-Metal Tunnel Diodes on Micro/Nano Antennas for Energy Harvesting and Detector Applications.* 2017 SBMO/IEEE MTT-S International Microwave and Optoelectronics Conference (IMOC), Aguas de Lindoia, 2017.
71. Donchev E., et al., *The rectenna device: From theory to practice (a review).* MRS Energy & Sustainability, 2014. **1**: p. 1-34.
72. Simmons J. G., *Generalized Formula for the Electric Tunnel Effect between Similar Electrodes Separated by a Thin Insulating Film.* Journal of Applied Physics, 1963. **34**(6): p. 1793-1803.
73. Simmons J. G., *Potential Barriers and Emission-Limited Current Flow Between Closely Spaced Parallel Metal Electrodes.* Journal of Applied Physics, 1964. **35**(8): p. 2472-2481.
74. Esaki L., *Discovery of he Tunnel Diode.* IEEE Transactions on Electron Devices, 1976. **23**(7): p. 644-647.
75. Poole C. and Darwazeh I., *Microwave semiconductor materials and diodes*, in *Microwave Active Circuit Analysis and Design*. 2016. p. 355-393.
76. Ridley, B.K. and T.B. Watkins, *The Possibility of Negative Resistance Effects in Semiconductors.* Proceedings of the Physical Society, 1961. **78**(2): p. 293-304.
77. Hashem, I.E., N.H. Rafat, and E.A. Soliman, *Theoretical Study of Metal-Insulator-Metal Tunneling Diode Figures of Merit.* IEEE Journal of Quantum Electronics, 2013. **49**(1): p. 72-79.
78. Khan A. A., et al., *Metal-insulator-metal diodes with sub-nanometre surface roughness for energy-harvesting applications.* Microelectronic Engineering, 2017. **181**: p. 34-42.
79. Periasamy P., et al., *Fabrication and characterization of MIM diodes based on Nb/Nb2O5 via a rapid screening technique.* Advanced Materials, 2011. **23**(27): p. 3080-3085.
80. Sanchez A., et al., *The MOM tunneling diode: Theoretical estimate of its performance at microwave and infrared frequencies.* Journal of Applied Physics, 1978. **49**(10): p. 5270-5277.
81. Krishnan S., *Design, Fabrication and Characterization of ThinFilm M-I-M Diodes for Rectenna Array*, in *Department of Electrical Engineering*. 2004, University of South Florida. p. 104.
82. Xia Y. and Whitesides G. M., Self-assembled Monolayer Films: Microcontact Printing. Encyclopedia of Materials: Science and Technology, 2001: p. 8309-8314.
83. Brown W. C., *The History of Power Transmission by Radio Waves.* IEEE Transactions on Microwave Theory and Techniques, 1984. **32**(9): p. 1230-1242.
84. Hashem I. E.,, Rafat N. H., and Soliman E. A., *Dipole Nantennas Terminated by Traveling Wave Rectifiers for Ambient Thermal Energy Harvesting.* IEEE Transactions on Nanotechnology, 2014. **13**(4): p. 767-778.
85. Pan Yi., et al., *Micro rectennas: Brownian ratchets for thermal-energy harvesting.* Applied Physics Letters, 2014. **105**: p. 253901.
86. Fumeaux C., Alda J., and Boreman G. D., *Lithographic antennas at visible frequencies.* Optics Letters, 1999. **24**(22): p. 1629-1631.
87. Fumeaux C., et al., *Nanometer thin-film Ni-NiO-Ni diodes for mixing 28 THz CO2-laser emissions with difference frequencies up to 176 GHz.* Journal of Applied Physics B, 1998. **66**(3): p. 327-332.

88. Gonzalez F. J. and Boreman G. D., *Comparison of dipole, bowtie, spiral and log-periodic IR antennas.* Infrared Physics & Technology, 2005. **46**: p. 418–428.
89. Jennings D. A., Petersen F. R., and Evenson K. M., *Extension of absolute frequency measurements to 148 THz: Frequencies of the 2.0- and 3.5-μm Xe laser.* Applied Physics Letters, 1975. **26**(9): p. 510-511.
90. Miskovsky N. M., et al., *Nanoscale Devices for Rectification of High Frequency Radiation from the Infrared through the Visible: A New Approach.* Journal of Nanotechnology, 2012. **2012**: p. 512379.
91. Collet, J. and D. Vuillaume, *Nano-field effect transistor with an organic self-assembled monolayer as gate insulator.* Applied Physics Letters, 1998. **73**(18): p. 2681-2683.
92. Wang Y. and L. M., *Growth of Ultrasmooth Octadecyltrichlorosilane Self-Assembled Monolayers on SiO2.* Langmuir, 2003. **19**(4): p. 1159-1167.
93. Wasserman S. R., et al., *The Structure of Self-Assembled Monolayers of Alkylsiloxanes on Silicon: A Comparison of Results from Ellipsometry and Low-Angle X-ray Reflectivity.* American Chemical Society, 1989. **111**: p. 5852-5861.